Journal of Materiomics 9 (2023) 683–700

Contents lists available at ScienceDirect

Journal of Materiomics

journal homepage: www.journals.elsevier.com/journal-of-materiomics/

Self-assembling nanoarchitectonics of low dimensional semiconductors for circularly polarized luminescence

Xiongbin Wang [a, b], Xuanyu Zhang [a], Huan Liu [a], Zikang Tang [b], Rui Chen [a, *]

[a] Department of Electrical and Electronic Engineering, Southern University of Science and Technology, Shenzhen, 518055, China
[b] Institute of Applied Physics and Materials Engineering, University of Macau, Avenida da Universidade, Taipa, Macau, 999078, China

ARTICLE INFO

Article history:
Received 2 December 2022
Received in revised form
23 January 2023
Accepted 29 January 2023
Available online 13 February 2023

Keywords:
Circularly polarized luminescence
Chirality
Low dimensional semiconductor
Self-assembly
Optoelectronics

ABSTRACT

Recently, the development of materials with circularly polarized luminescence (CPL) has attracted numerous attentions owing to their potential applications in various fields. Among diverse mechanisms for the origin of chiroptical properties in low dimensional semiconductors (LDS), the self-assembly approach provides a powerful technique for acquisition of strong chiroptical activity. Benefiting from this approach, LDS could be endowed with CPL in which the dissymmetry factor, a vital parameter for evaluating the performance of CPL, could be greatly improved. In this review, state-of-the-art of self-assembled LDS will be summarized. The current challenges and perspectives in this emerging field are also presented. This review could not only provide insights of the fundamentals of self-assembled chirality, but also shine light for designing CPL-active functional nanomaterials toward their applications based on novel optoelectronic devices.

1. Introduction

Circularly polarized light has aroused tremendous attentions due to its potential applications including three-dimensional display, spintronics information encryption and optical sensors [1–3]. Through the combination of linear polarizer and quarter waveplates, circularly polarized light with different handedness can be obtained from an unpolarized light. However, this method causes huge energy loss during the modulation [4]. Circularly polarized luminescence (CPL) is an optical phenomenon that describes the difference of emission intensity between left-handed circularly polarized light (LCP) and right-handed circularly polarized light (RCP) from chiral luminophores. Using CPL-active materials as light source could prevent the drawback of energy loss. Therefore, it is urgent to explore novel CPL-active materials for various applications. Notably, with well-defined chirality, *i.e.*, chiral carbon atoms, chiral organic emitters are frequently considered as CPL sources [5]. However, chiral organic emitters usually possess relatively low luminescent dissymmetry factor g_{lum} which restricts their potential applications [4]. The prospect of using low dimensional inorganic materials for CPL generations has flourished in the past decade due to the huge potential to enhance and adjust the CPL signal through tunable electronic states and geometries of the overall configurations [6,7]. However, with the rapid development of CPL-active materials, novel optoelectronic materials with exotic photo and electro physical effects are on augmenting demand. In light by this requirement, low dimensional semiconductors (LDS) such as perovskites, CdSe quantum dots, carbon dots and nanorods *etc.* have aroused extensive attractions due to their unique and excellent properties. This review is going to focus on self-assembled LDS with CPL response.

In principle, chiral LDS can be classified into three categories according to the synthetic strategies: a) LDS with intrinsic chiral space groups or lattice [8], b) LDS with chirality induced by chiral capping ligands [9], and c) self-assembled structures of LDS with asymmetric features [1,10,11]. Among different construction strategies, the self-assembly technique not only demonstrates strong structure control capability, but also enhances the desired CPL signals. Moreover, LDS could be easily endowed with CPL property through self-assembly approach no matter whether they have chirality or not. By the virtue of geometry-tailored CPL behaviors and relatively high anisotropic factors g_{lum}, chiral assemblies of LDS are among the most promising approaches for the fabrication of chiral LDS. Therefore, it is imperative to understand and further control the assembly of LDS building blocks in a chiral manner.

* Corresponding author.
E-mail address: chenr@sustech.edu.cn (R. Chen).
Peer review under responsibility of The Chinese Ceramic Society.

https://doi.org/10.1016/j.jmat.2023.01.009

The research on CPL-active assembled structures of LDS develops rapidly with many emerging potential applications. Herein, in this review, recent progresses on chiral assemblies of LDS with CPL activities in terms of their synthesis, CPL responses and possible mechanisms for modulation of CPL signals for optoelectronic applications will be emphasized (Fig. 1). Particularly, in Section 2, CPL spectroscopy is briefly introduced with special attention to the fundamental mechanism and possible origin of artifacts. Then, fundamental principles on design strategies of chiral assemblies of LDS are highlighted in Section 3. After that, applications based on CPL-active assembled LDS are introduced in Section 4. Finally, challenges and perspectives in this area will be discussed which might provide timely insights for researchers in developing novel assembled LDS with high quality.

2. CPL spectroscopy: Basic concepts and artifacts

2.1. Basic concepts of polarization and CPL

Light is an electromagnetic wave with coupled electric and magnetic fields which are perpendicular to each other. Generally, the polarization of light is related to the oscillating direction of the electric field. Natural light and many other commercialized light sources are unpolarized light that consists of waves with an equal mixture of polarizations. Polarized light is generally divided into three different types, namely, linearly, circularly and elliptically polarized, respectively. Considering two planar waves, it is not complicated to figure the configurations out. A linearly polarized light is composed of two planar waves without phase difference in which electric field oscillate in a single direction. Two perpendicular planar waves with different amplitudes and phase quadrature could form an elliptically polarized light. Circular polarization could be regard as a limiting case of elliptical polarization in which the two planar waves should have equal amplitude and differ in phase by 90°. Obviously, two possible senses would occur in a circularly polarized light. If the electric field vector rotates in a clockwise manner with respect to the propagate direction, this light is called as RCP. In comparison, LCP has the electric field vector that rotates counterclockwise. Usually, an unpolarized light could transform to linearly polarized light after passing through a linear polarizer. Meanwhile, a linearly polarized light could be converted to circular polarized light by placing a quarter-waveplate in front of it with the angle between the waveplate axes and the polarization axis fixed at 45°, while a circularly polarized light could convert to linear polarized after passing through a quarter-waveplate (Fig. 2a) [12]. The main drawback of this approach for producing circularly polarized light is the significant energy loss during the modulation.

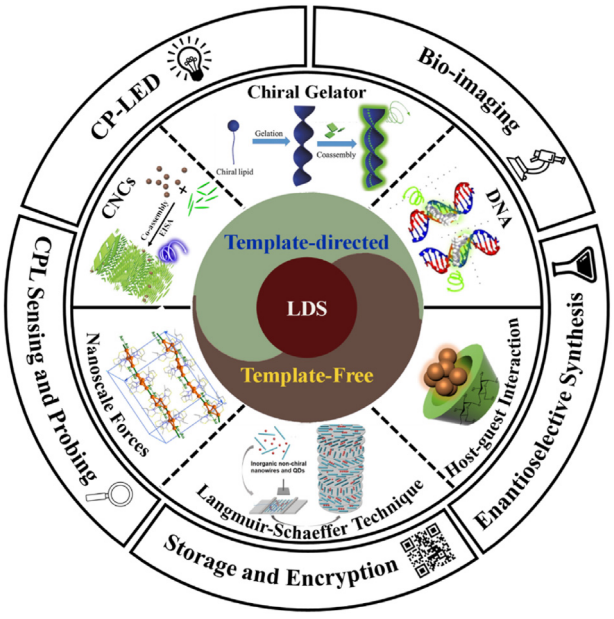

Fig. 1. Schematic representation of assembly strategies of LDS with emphasis on templated-directed and template-free guided assembly. Different applications based on assembled LDS are also presented.

In a chiral system, circularly polarized light could be absorbed and emitted corresponding to CD and CPL processes, respectively (Fig. 2b) [13,14]. Based on these concepts, CPL is defined as differential spontaneous emission of left-handed (I_L) and right-handed (I_R) circularly polarized radiation for chiral luminescent systems photoexcited by an unpolarized light:

$$\Delta I = I_L - I_R \tag{1}$$

Usually, g_{lum} is used to evaluate the degree of circular polarization since the absolute emission intensity is difficult to measure. It is defined as the ration of the difference of CPL intensity divided by average total emission intensity, which could be expressed as follow:

$$g_{lum} = \frac{2(I_L - I_R)}{I_L + I_R} = \frac{2\Delta I}{I_{total}} \tag{2}$$

Clearly, the g_{lum} is a value in the range from +2 to −2, which corresponds to complete left-handed polarization and right-handed polarization, respectively. The chiral luminescent system shows no circular polarization when the g_{lum} is zero.

CPL spectroscopy is the emission analog of circular dichroism (CD) spectroscopy which is defined as the difference of absorption of LCP and RCP, that is:

$$g_{abs} = \frac{2(\varepsilon_L - \varepsilon_R)}{\varepsilon_L + \varepsilon_R} = \frac{\Delta\varepsilon}{\varepsilon} \tag{3}$$

where ε_L and ε_R are the molar absorption coefficients for LCP and RCP, respectively. ε denotes the average quantity of the molar absorption coefficients, which is directly related to samples. For emitting molecules with isotropic orientation distribution, CD and CPL share the same theoretical expression for the molecular properties. Typically, for an electronic transition $i \rightarrow j$, both CPL and CD could be estimated by one single parameter related to molecular properties, which is known as *rotation strength*, and could be express as follow:

$$R_{ij} = Im\left(\vec{\mu}_{ij} \cdot \vec{m}_{ij}\right) \tag{4}$$

where $\vec{\mu}_{ij}$ and $\vec{m}_{ij}$ are the electric and magnetic dipole moment vectors, respectively [15]. It should be pointed out that the magnitude and sign of the rotation strength might be different for CD versus CPL. CD provides the ground states information while CPL shows both configurational and conformational properties of chiral system in its excited states, in which the dipole moment vectors possess different compositions [15,16]. More specifically, g_{lum} is proportional to the rotation strength and inversely proportional to the transition oscillator strength $|D_{ij}|$ [17,18]. The value of g_{lum} is often evaluated by follow expression:

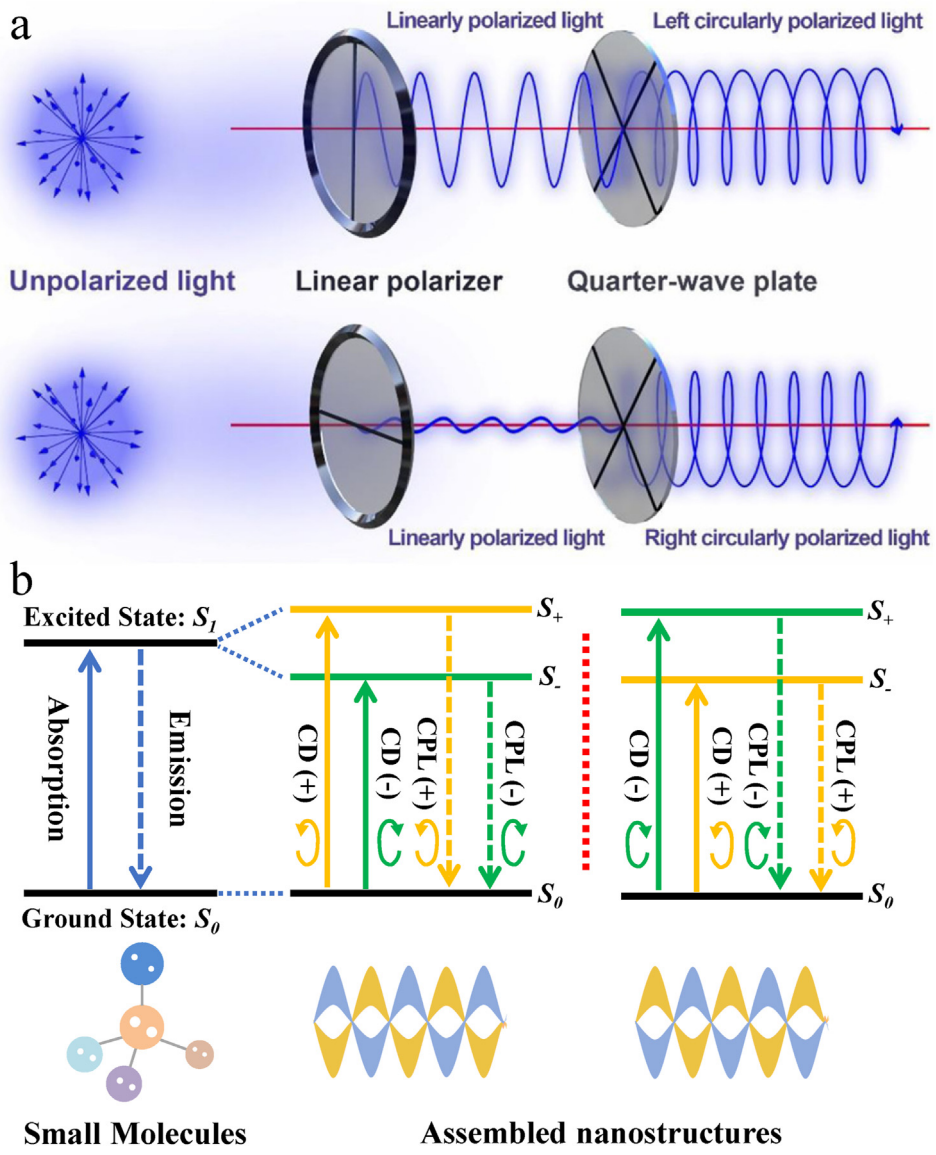

Fig. 2. (a) Schematic diagram of LCP and RCP generation. Reproduced with permission from Ref. [12]. Copyright 2021, Wiley-VCH. (b) Schematic illustration of CD and CPL processes in molecules and their assembled nanostructures.

$$g_{\mathrm{lum}} = \frac{4R_{ij}}{|D_{ij}|} = 4Re\left[\frac{\vec{\mu}_{ij}\cdot\vec{m}_{ij}}{\left|\vec{\mu}_{ij}\right|^2 + \left|\vec{m}_{ij}\right|^2}\right] \tag{5}$$

In the case of electric dipole allowed transition in which the electric dipole moment vector is much larger than the magnetic dipole moment vector, g_{lum} could be approximated to follow equation:

$$g_{\mathrm{lum}} = 4\frac{\left|\vec{m}_{ij}\right|\cos(\theta)}{\left|\vec{\mu}_{ij}\right|} \tag{6}$$

where θ is the angle between the dipole moment vectors. From the above equation, a system shows no CPL signal when its electric and magnetic dipole are perpendicular to each other. One might obtain high g_{lum} when the system has electric dipole-forbidden and magnetic dipole-allowed transitions. However, the observed luminescence is usually very weak in this case if no other photophysical mechanism contributes to the emission [17].

The physical quantity g_{lum} is insufficient to evaluate the overall performance of a circular polarized emitter since it only considers the characters of the imbalance of circularly polarized light during the emission process. To solve this problem, Tang's group introduces a new parameter to evaluate the performance of CPL-active emitter. The figure of merit (FM) is defined as the product of emission quantum yield (∅) and g_{lum}:

$$\mathrm{FM} = \varnothing \times g_{\mathrm{lum}} \tag{7}$$

It could be seen than *FM* would reflect comprehensive quality of a CPL-active emitter [19]. Theoretically, the maximum of ∅ is 1, and absolute value of g_{lum} is 2, the *FM* for an ideal CPL-active system is 2. To extract a higher FM value, a large g_{lum} and a high ∅ should satisfy simultaneously [13]. Similarly, Arrico *et al.* introduce a

metric analogy with fluorescence brightness (B) defined as the product of ∅ and molar extinction (ε_λ) measured at excitation wavelength to evaluate the circularly polarized emitter [17]. The brightness for CPL is defined as:

$$B_{\mathrm{CPL}} = \varepsilon_\lambda \times \varnothing \times \frac{g_{\mathrm{lum}}}{2} = B \times \frac{g_{\mathrm{lum}}}{2} \tag{8}$$

From the above equation, it is found that the brightness for CPL ingrates the main photophysical parameters of circularly polarized emitters. Besides, the quantity could be used for direct comparison among different CPL systems. However, this metric is only applicable to sample in solutions. To discuss the supramolecular, aggregated and solid states samples, a more general definition has been proposed by Tanner *et al.* and could be expressed as [20]:

$$B' = \varepsilon_{\mathrm{abs}} \times \varnothing \tag{9}$$

where $\varepsilon_{\mathrm{abs}}$ is the absorption efficiency which is equal to the number of absorbed photons divided by incident ones. Then, the brightness for solid state sample could be rewritten as:

$$B'_{\mathrm{CPL}} = \varepsilon_{\mathrm{abs}} \times \varnothing \times \frac{g_{\mathrm{lum}}}{2} = B' \times \frac{g_{\mathrm{lum}}}{2} \tag{10}$$

2.2. Artifacts in CPL measurements

Since the first observation of CPL from chiral crystal of sodium uranyl acetate reported by Samoilov in 1948 [21], the detection of CPL depends on home-made instruments for a long time. For most samples, the magnitude of the circularly polarized component from emitted light is usually much lower than the total emission intensity. Under this circumstance, the intrinsic CPL signal would be easily covered up by spurious signals. Therefore, in order to obtain intrinsic CPL, careful consideration should be given to eliminating parasitic signals.

The measurement of CPL is based on the polarization modulation technique, and some artifacts may occur due to the imperfection of optical elements. There are mainly two sorts of instrumental artifacts which would affect the detected CPL signals. Photo-elastic modulator (PEM) is an important optical element for collecting CPL signals. Due to the residual static birefringence of PEM, a parasitic signal would be generated when the linear polarization of emitted light interferes with the PEM [22]. The parasitic signal may have comparable order of magnitude with the intrinsic CPL signal even if the stray birefringence of PEM is very small. Nevertheless, parasitic signal from PEM is depended on the angle between the sample and the optical axis. The artifact could be revealed by a simple rotation of samples about optical axis. Another artifact related to the instrument comes from the second harmonic response of the lock-in amplifier which is used for transducing the electric signal [23]. Usually, the linearly polarized luminescence signal is measured at 100 kHz while the CPL is detected at 50 kHz during the lock-in detection which might cause artifact signal [24].

Apart from artifacts from instruments, the presence of linear polarization in the emitted light comes from photo-selection effect, which was firstly observed by Gafni and Steinberg, would contribute to the recorded signal [25]. The photo-selection effect could be understood that the orientation distribution of the emitters depends on the absorption dipole moment with respect to the direction and polarization of excitation light. This effect makes it difficult to detect CPL due to presence of linear polarized component of the emitted light. The photo-selection effect could be eliminated by the use of combinations of excitation/emission geometries. For isotropic samples, the photo-selection effect can be ignored. It is recommended that depolarized light should be used for excitation when adopting a 0- or 180-degrees geometry. When choosing a 90° geometry, the liner polarized excitation should be parallel to the detected direction. Alternatively, the so-called "magic angle" instrumental setup could also be used for gathering CPL [26]. It is very important to ensure that the samples are isotropic in the plane perpendicular to the emission detected direction, so as to make sure that the CPL is only related to the rotation strength and translation dipole strength. Recently, Harada *et al.* develop an analytical method based on Mueller matrix for altering intrinsic CPL signal, which could rule out the influence of parasitic artifacts owing to linear polarization [27].

When the CPL band is too close to the CD band or even overlaps with it, part of the fluorescence would be reabsorbed by the emitters while the reabsorption is different between right-handed and left-handed CPL. Therefore, the observed CPL need to be revised. Fortunately, analytical method for removing the artifact has been proposed [22,28]. The corrected CPL could be expressed as:

$$CPL_{\mathrm{Corr}} = \frac{I_{\mathrm{Obs}}}{T}(\alpha \bullet \ln(10) \bullet \Delta A) + \frac{CPL_{\mathrm{Obs}}}{T} \tag{11}$$

where I_{Obs} and $\mathrm{CPL}_{\mathrm{Obs}}$ are the observed emission and CPL signal, respectively. T represents the observed transmittance. α is the function of sample's optical density at excitation wavelength. ΔA is the CD signal. Detail discussion about the corrected CPL could be found in literatures [22,28,29].

Generally, the influence of emitted light scattering should be taken into consideration for solid samples and viscous media [22]. When scattering is predominant and the spectra of circular differential scattering (CDS) overlaps with CPL bands, the CDS might manifest itself as apparent CPL. Different with CPL, the characteristics of CDS including intensity, wavelength and ellipticity would be significantly impressed by the geometry, chirality and orientational distribution of emitters [30]. CPL might be severely affected by CDS. Due to the influence of CDS, CPL signal show sign-reversal upon increasing the thickness of film [31]. Unexpected and strong dependence of g_{lum} of films have been observed for a long time. However, this phenomenon is recently rationalized on the basis of CDS after ruling out possible artifacts using Muller matrix ellipsometry as reported by Wan *et al.* [31].

In conclusion, obtaining intrinsic CPL should be considered cautiously since many serious artifacts could appear in the signal especially for solid-state samples. The reproducibility of data in different samples should be carefully checked to eliminate the influence of artifacts. Some protocols have been suggested for acquiring CPL spectra, and one can refer to literatures if needed.

3. CPL from self-assembled structures

3.1. Self-assembly of LDS directed by soft templates

Many pre-existing structures could be used as templates for the assembly of LDS. Templates are regarded as substrates that could provide many active sites for binding target LDS when achieving the self-assembly process. It has been realized that templates-assist assembly is a simple and effective method because it exhibits very high preparation efficiency, regulable morphology and excellent ability. Many soft templates created by molecules such as DNA, gel and cellulose nanocrystals (CNCs) play a vital role in organizing LDS. In the past decade, various synthesis protocols based on soft templates for LDS assembly have been demonstrated. In this section, the assembly of LDS directed by soft templates will be presented.

3.1.1. Assembly of LDS templated by DNA and G-quartet complex

In the past decade, DNA nanotechnology has experienced extensive development. It provides a novel and excellent route for the chiral assembly of nanomaterials in which DNA molecules are relatively stable and could be easily modified [32]. DNA origami which is the nanoscale folding of DNA for creating 2-dimensional and 3-dimensional objects has been used for directing the assembly of nanoparticles (NPs) with different chiral structures, such as dimer, pyramid and helices [33–35]. For instance, four different NPs (three Au NPs with different sizes and a quantum dots (QDs)) could assembly into chiral pyramid structure by DNA origami [34]. The obtained pyramid structure shows extensive optical activity in visible range. By using a DNA origami 24-helix bundle as template, Au NPs with a diameter of 10 nm are attached to the surface of the bundle forming a twist structure (Fig. 3a. The handedness of the helix could be easily adjusted by the sequence of DNA). The Au NPs helices display bisignate CD signal, with its peak near the plasmon resonance frequency, which is completely consistent with the calculated CD signal [35]. Although plenty of studies on the assembly of plasmonic NPs with strong CD response have been reported, it is expected that DNA origami can be used as template to realize the assembly of luminescent NPs which will generate CPL.

Classical double stranded DNA (dsDNA) consisted with two polynucleotide chains could be used as a matrix for providing a chiral environment that enable chirality transfer from DNA to luminophore. Gorecki's *et al.* investigate the interaction between calf thymus DNA and thiazole orange (TO) which is a common fluorescent stain for DNA [36]. The hybrid system exhibits induced CD signal in the absorption band of TO molecules as well as CPL signal in the emission band. Since the TO molecule is achiral, and the helical dsDNA does not absorb visible light, the chirality transfers from dsDNA into TO molecules. These findings provide new insights into the application of CPL in the detection of DNA and other bio-compounds. Apart from this example, Ding's group successfully realizes the co-assembly of cyanine molecules, which are fluorophores of aggregation induced emission and chiral dsDNA [37]. The DNA-cyanine complex shows strong CPL response. Typically, the cyanine molecules will bind to the groove of DNA through simple electrostatic attraction. After examining duplex DNA templates with different ratios of guanine/cytosine, the cyanine dyes prefer to bind to AT-rich region among the dsDNA. This result is also supported by theoretical calculation. The dsDNA could not only confine the intramolecular rotation of the molecule which significantly enhance the emission, but also transfer the chirality from itself to the cyanine dye. Therefore, the assembly features a remarkable CPL in correspondence to the emission band of achiral cyanine dye (Fig. 3b). In addition, DNA-based nanoswitches with conformational changes related to pH are employed as assembly template. The switchable DNA strands would transfer into intramolecular triplex structure with the relative content of TAT/CGC triplets in the DNA switches determining the pH responsive ranges. When pH value changes from 8 to 5, the DNA templates transit from duplex to triplex, which results in a tunable chiroptical signals. These results exhibit enormous potential for constructing CPL-active nanoassemblies by using dsDNA as template.

G-quartet, composed of planar association of four guanines by a Hoogsteen bond, is widespread in human genome [38]. The most famous one is G-quadruplex (G4) DNA. Noncanonical G4 DNA could also be used as templates to construct CPL-active materials. Different with classic DNA, G4 structures could be regarded as a four stranded helical DNA consisting stacks of G-quartets [39]. Recently, G-quarters have aroused extensive attention in multidisciplinary fields including pharmaceutical chemistry [40], supramolecular chemistry [41] and nanotechnology [42]. Chen *et al.*

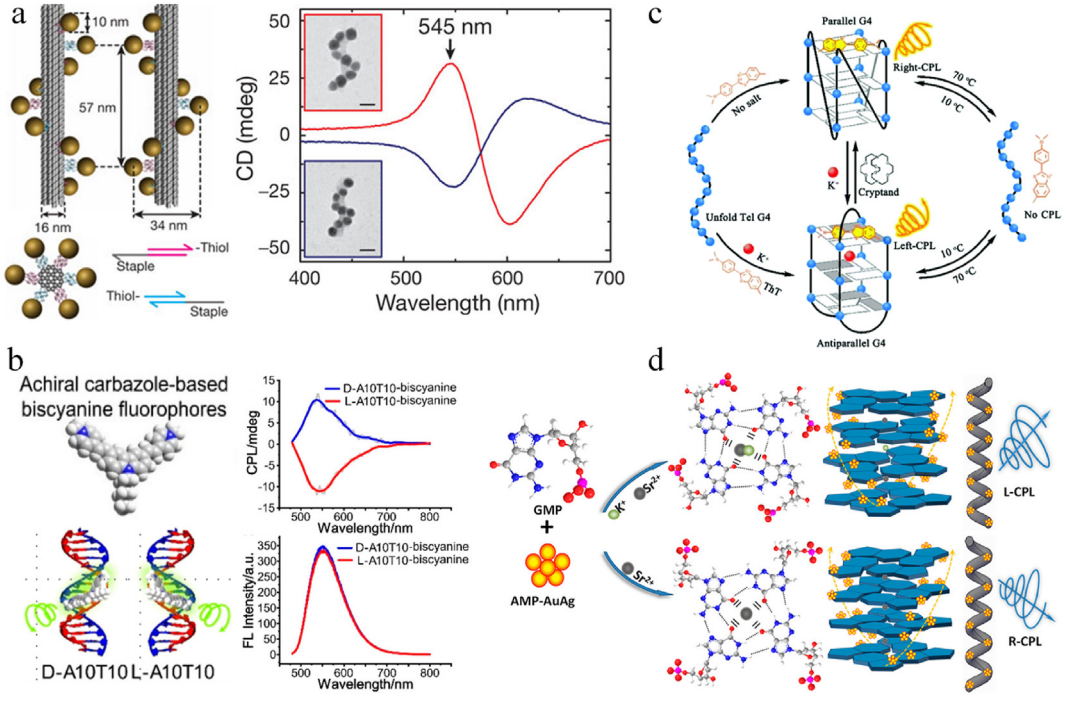

Fig. 3. (a) Au NPs helices with left and right handedness (left). CD spectra of the corresponding nanohelices (right). Reproduced with permission from Ref. [35]. Copyright 2012, Macmillan Publishers Ltd.. (b) Left: schematic illustration of achiral biscyanine fluorophores and DNA-cyanine assembled structure. Right: mirror CPL spectra and emission spectra of D- and L-DNA duplex–biscyanine complex. Reproduced with permission from Ref. [37]. Copyright 2019, The Royal Society of Chemistry. (c) Scheme of co-assembly of ThT dye and human telomeric G4 DNA. The CPL signal could be regulated by salt and temperature. Reproduced with permission from Ref. [38]. Copyright 2019, The Royal Society of Chemistry. (d) Scheme of the self-assembly of the G-quartet nanofiber and bimetallic AuAg nanoclusters with CPL response. Reproduced with permission from Ref. [43]. Copyright 2020, The American Chemical Society.

successfully realize the CPL from achiral dye thioflavin T (ThT) by using human telomeric G4 as template in which the chirality is transferred from the template to the binding dye (Fig. 3c) [38]. After analyzing different DNA sequences and structures, it is found that left-handed CPL is induced by the antiparallel G4 structures while the right-handed CPL is originated from parallel G4 framework. Intriguingly, the G4 structure can transfer from parallel into anti-parallel by adding K^+ resulting an inversed CPL signal. In addition, the CPL signals could be easily regulated by temperature. When temperature increase from 10 to 70 °C, the G4 conformation would be destroyed. After annealing, the structure would be reconstructed. Therefore, the CPL signal from the hybrid system would change from active to inactive with temperature. Reported by the same group, a guanosine derivative named as 5′-guanosine monophosphate (GMP) is used as template for the assembly of dye [39]. Surprisingly, the helical handedness of the assembled nanofiber could be well regulated by metal ions. Typically, left-handed helical G-quartet nanofiber would be obtained by the assembly of GMP and Sr^{2+} while right-handed nanofiber is obtained when K^+ ion is added into the mixture of GMP and Sr^{2+} (Fig. 3d). The Sr^{2+} is used as stabilizer and initiator during the assembly process. Different achiral dyes are used for the co-assembly of the helical nanofiber with strong CPL responses covering the entire visible spectrum. The g_{lum} could reach up to 10^{-2}. Metal nanoclusters (MNCs) are novel nanomaterials composed of several hundreds of atoms, which have unique optical properties. Different from their bulk materials, MNCs have precise atomic structure and discrete energy levels. MNCs could be simply obtained by one-pot approach with high photoluminescence quantum yield that makes them superior than traditional organic dyes. Benefiting from the powerful affinity between MNCs and nucleotides, adenosine 5′-monophosphate (AMP) is used for stabilizing gold-silver bimetallic nanoclusters [43]. By the co-assembly of AMP-AuAg nanoclusters and G-quartet nanofiber, strong CPL response could be obtained with g_{lum} around 10^{-2}.

3.1.2. Chiral gelators guided assembly

Supramolecular organogels are known as soft materials composed of low-molecular-mass organogels and hydrogels [44]. Some organic molecules named gelators could self-assemble into a three-dimensional network which is driven by non-covalent interaction such as hydron bond, π-π interaction, electrostatic interaction and van der Waals forces to form supramolecular gels [45]. Benefiting from supramolecular chemistry, the function and properties of supramolecular gels could be easily tuned by designing the gelators. By introducing chiral unit in the gelators, chiral gel could be prepared. Recently, chiral supramolecular gels have been used as template to achieve the assembly of achiral fluorophore for CPL [13]. The handedness and intensity of the induced CPL could be easily regulated by adjusting the interactions and position of the fluorophore on the gels. Besides, according to the properties of the gelators, the obtained assemblies would show different structures such as nanofibers [46], nanoribbons [47] and nanotubes [48].

Hybrid metal halide perovskites exhibit outstanding optical and electronic properties which have been the forefront in numerous research fields. Endowing perovskites with CPL would inspire tremendous innovative applications. Duan's group report that achiral perovskites could co-assemble with chiral gelator in nonpolar solvent (Fig. 4a) [48]. In a detail process, oleic and oleylamine capped perovskite ($CsPbX_3$ (X = Cl, Br and I)) is mixed with amine-containing lipid (LGAm/DGAm). It is found that the mixture dissolved in hexane could form co-assemblies without quenching the emission of perovskite. In addition, the obtained co-assemblies show mirror image CPL signals with maximum g_{lum} up to 7.3 × 10^{-3} depending on the handedness of the chiral lipid. The emission of the perovskite could tune from red to blue by simply changing the precursor from I to Cl. Therefore, the CPL of the co-assemblies can cover visible range from 410 to 600 nm. When heating the cogel, the structure of the co-assemblies would be destroyed which leads to CPL silent signal. As a result, the chirality of the achiral perovskite has been ascribed to the chiral arrangement of the nanomaterials in the self-assemble chiral networks. Lanthanide-doped up conversion nanoparticles (UCNPs) is another kind of promising inorganic nanomaterials which can convert near-infrared (NIR) radiative light into visible or ultraviolet (UV) light. This property makes them useful in many biological applications such as bioimaging and biosensing. Also reported by Duan's group, achiral UCNPs could be helically encapsulated into chiral gel assembled from the chiral lipid gelator (LGAm/DGAm) (Fig. 4b) [49]. The co-assemblies exhibit upconverted CPL (UC-CPL) when they are excited by a 980 nm laser. To confirm the mechanism of the induced CPL, two comparison experiments are conducted. When the mixture of UCNPs and gelator is dissolved in chlorobenzene, no CPL could be detected, which indicates that the assemble state is very important for CPL. In addition, no CPL can be observed when using achiral BAm molecules which possess similar structure with the chiral gelator (LGAm/DGAm). Therefore, the chiral arrangement of UNCPs along the chiral nanotube is crucial for the induced UC-CPL. Similarly, Cao *et al.* synthesize a pair of chiral amphiphilic gelator (*D*/*L*-MA-ALA-COOH) which could form chiral gel with helical morphology in nonpolar solvent due to the intermolecular hydrogen bonds in the carbonyl and amide group [50]. The chiral gel could be used as template for the assembly of achiral $CsPbX_3$ perovskites with induced CPL signal whose g_{lum} reaches up to 8.2 × 10^{-3}.

Apart from achiral luminophore, chiral luminophore has also been used for assembly using gel as template. Hao *et al.* choose the well-known gelator N-(9-fluorenylmethoxycarbonyl)-protected glutamic acid (Fmoc-Glu) and chiral lysine (Lys) as building blocks to realize the chiral assembly of FeS_2 QDs with $|g_{lum}|$ of 0.06, which is 10–100 times larger than those CdSe QDs capping with chial amino acids (Fig. 4c) [46]. Particularly, chiral FeS_2 QDs is obtained using L/D-cysteine (L/D-Cys) as capping ligand in which the Cys molecules could modify the surface of FeS_2 *via* strong iron-sulfur bonds. Benefiting from the enriched carboxylate groups of the gelators and the amine groups of FeS_2 QDs, cogels could be formed through electrostatic interaction. Observed from SEM images, the obtained cogels have helical morphology. More importantly, the cogels display mirror-imaged CPL signals at 496 nm corresponding to different handedness of the nanofibers. It is concluded that the chiral arrangement of chiral FeS_2 is crucial for the chirality transfer mechanism. Surprisingly, the hydrogel would exhibit abnormal behavior when illuminated with CPL. When D-(Gel + FeS_2) is illuminated with LCP, the gel would have an expended helical pitch while shortening helical can be observed when D-(Gel + FeS_2) is illuminated with RCP. Similar tendency has also been observed for L-(Gel + FeS_2). The shortening and expended helical pitch would influence the coupling between the QDs and gelators resulting in variant CD and fluorescence. Although the authors do not show the CPL signal of the cogels after illuminated with CPL, it can be predicted that the CPL of the cogels will be different from the previous one. This research provides valuable insight for amplification and modulation of chirality in soft matter and functional nanomaterials.

3.1.3. CNCs templated assembly

CNCs are well-known renewable and biocompatible nanomaterial which could be extracted from bulk cellulose. In the past decades, different methods have been developed to prepare CNCs such as acid hydrolysis, enzymatic hydrolysis, oxidative

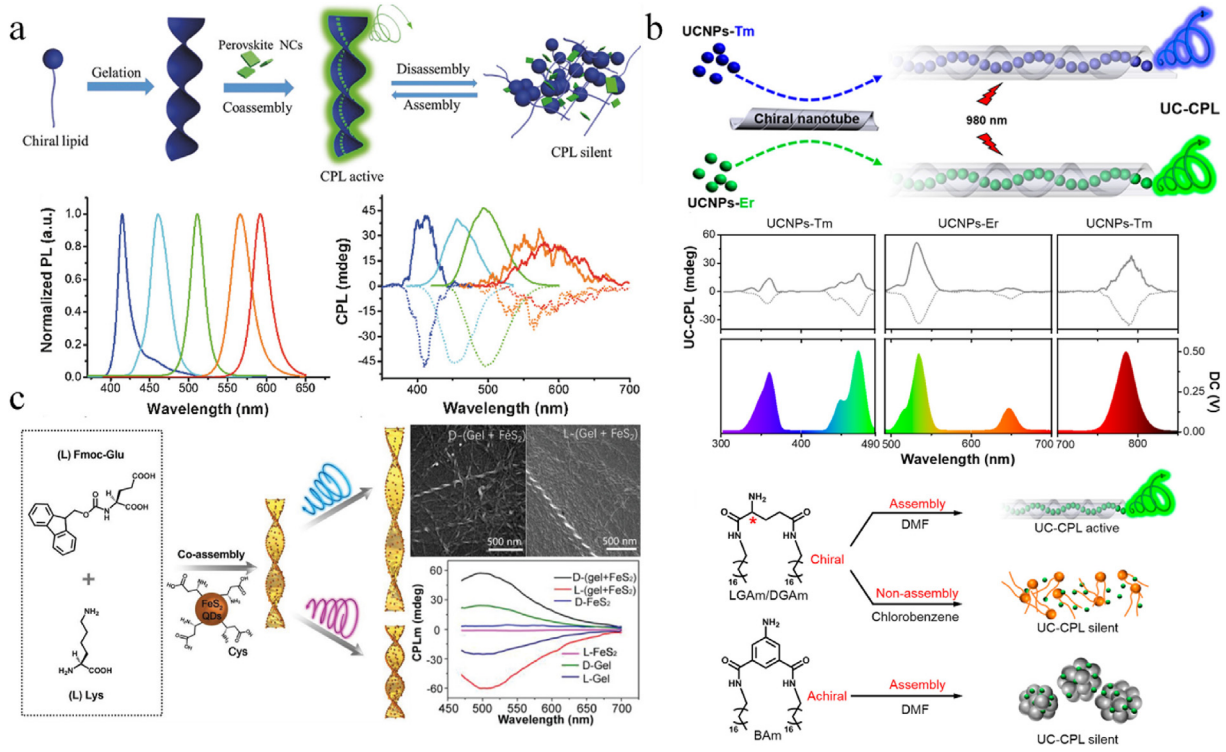

Fig. 4. (a) Schematic of the co-assembly induced chirality of perovskites in chiral gel (Top). Photoluminescence spectra of $CsPbX_3$ with different compositions doped in DGAm (Bottom left). Mirror-imaged CPL spectra of corresponding co-assembly gel (excited at 310 nm) (Bottom right). Reproduced with permission from Ref. [48]. Copyright 2018, Wiley-VCH. (b) Top: illustration of the co-assembly of achiral UCNPs and chiral nanotube with induced CPL. Upon excitation of 980 nm laser. Middle: Mirror-imaged UC-CPL spectra and photoluminescence spectra of the chiral nanotube doped with different UCNPs. Bottom: possible mechanism for the UC-CPL. Chiral gelators would form chiral assembly state in DMF resulting an induced CPL for UNCPs while the un-assembled state generates silent CPL signal. Achiral BAm shared similar structures with D/LGAm also display zero CPL signal. Reproduced with permission from Ref. [49]. Copyright 2019, American Chemistry Society. (c) Illustration of the co-assembly from chiral gelators and chiral FeS_2 QDs with CPL response. Right: SEM images of the helical nanofibers. Mirror-imaged CPL spectra (Bottom right). Reproduced with permission from Ref. [46]. Copyright 2019, Wiley-VCH.

degradation and ionic liquid [51]. Acid hydrolysis has become the most commonly used chemical method for the preparation of CNCs due to its advantages of simple operation, low cost and easy availability of raw materials. CNCs obtained from acid hydrolysis have rod-like morphology which could self-assemble into left-handed chiral nematic structures when the concentration of CNCs reaches a critical value [52]. The assembled structure could selectively reflect CPL. The wavelength of the selective reflection satisfies Bragg equation [53]:

$$\lambda_{\text{centered}} = nP\sin(\theta) \tag{12}$$

where n is the refractive index of the structure, P is the helical pitch, and θ is defined as the angle between incident light and surface of the film. The intriguing properties of CNCs make them a promising template for implementing the chiral assemble of NPs.

Silicon (Si) QDs are potential candidates in various fields because of their photostability and nontoxicity [54,55]. We have successfully realized the chiral assembly of water-soluble Si QDs guided by CNCs (Fig. 5a) [56]. The positively charged Si QDs could attach on the surface of CNCs *via* electrostatic interaction. The mixture could form chiral nematic structures during the evaporation induced self-assembly (EISA) process. When excited at 350 nm, the chiral photonic crystal films display very strong right-handed CPL response with a maximum $|g_{\text{lum}}|$ up to 0.25, which is much larger than ligand induced NPs and assembly NPs templated by gelators. The CPL of the photonic crystal films could be tuned by varying the concentration of Si QDs resulting different helical pitches. Photonic band gap (PBG) should simultaneously consider with the emission band of Si QDs for understanding the CPL behavior. Largest g_{lum} could be obtained when PBG totally coincides with the emission band. Similar to Si QDs, fluorescent carbon QDs which are also promising nanomaterials have aroused numerous attentions [53]. Many efforts have been devoted to acquiring luminescent carbon QDs with CPL response [57–59]. By mixing carbon QDs with CNCs suspension, Xu's group successfully fabricates chiral nematic films with strong CPL response (Fig. 5b). The $|g_{\text{lum}}|$ of the freestanding film could reach up to 0.74 [53]. The wavelength of the freestanding films could be tuned from near UV to NIR region by the choice of carbon QDs and the change of PBG.

In 2020, Liu's group, for the first time, observe CPL and circularly polarized room-temperature phosphorescence (CPRTP) in hybrid photonic films from the co-assembly of CNCs, poly(vinyl alcohol) (PVA) and carbon QDs (Fig. 5c) [60]. When excited under UV light, the hybrid film CPL while CPRTP could be observed after removing the excitation light. The functional groups on the QDs would produce triplet excitons which are stabilized by the hydrogen bonding networks of the chiral photonic films leading to CPRTP with long lifetime. Both the CPL and CPRTP could be facilely regulated by the PBG including intensity and handedness. For instance, right-handed CPL is observed when the emission band of carbon QDs locates in the middle of PBG. In contrast, left-handed CPL could be induced when the PBG is far away from the emission band.

Apart from isotropic QDs, CNCs could also be employed as soft template to guide the assembly of anisotropic NPs. By doping CdSe/CdS core-shell quantum rods (QRs) into CNCs, Shi *et al.* fabricates chiral nematic composite film with iridescent colors. The optical activity of the composite film could be manipulated by adjusting the relative position of the PBG and emission band of QRs [52]. The

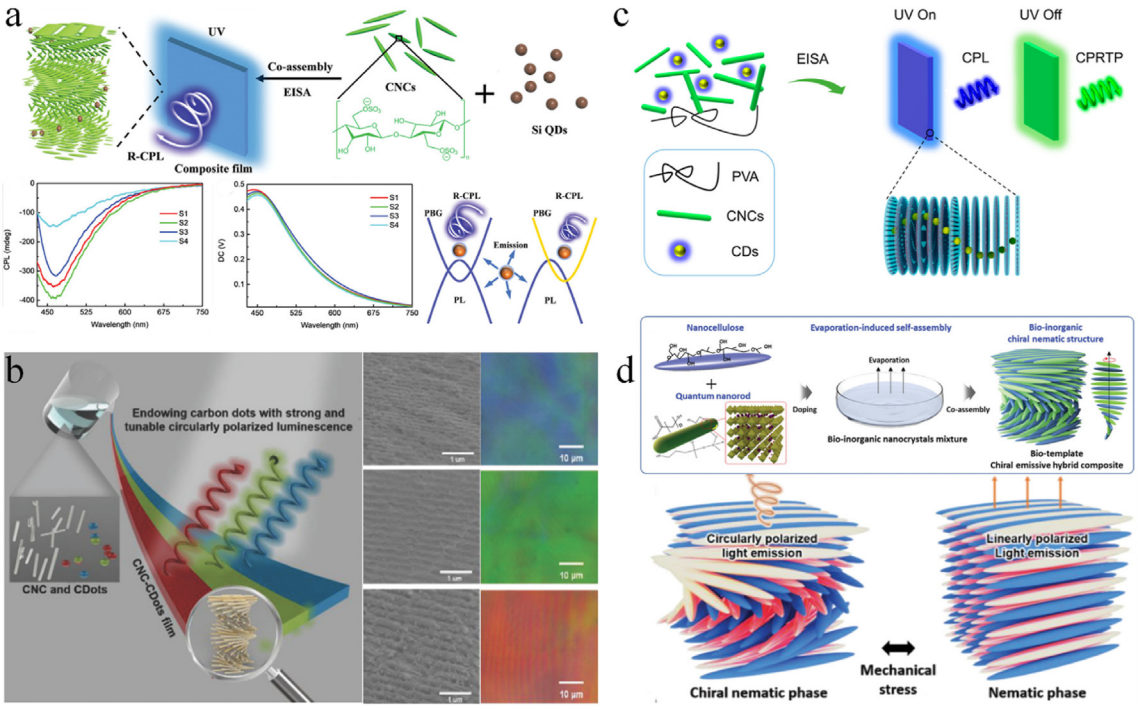

Fig. 5. (a) Schematic of the co-assembly of CNCs and Si QDs. When excited by UV light, the obtained films exhibit right-handed CPL. The intensity of CPL is determined by PBG of the freestanding film and emission band of Si QDs. Reproduced with permission from Ref. [56]. Copyright 2022, Wiley-VCH. (b) Illustration of the EISA of CNCs and carbon QDs exhibiting tunable CPL. Right: SEM images and POM images of different composite films. Reproduced with permission from Ref. [53]. Copyright 2018, Wiley-VCH. (c) CPL and CPRTP from chiral photonic films fabricating from PVA, CNCs and carbon QDs through EISA process. Reproduced with permission from Ref. [60]. Copyright 2020, American Chemical Society. (d) Illustration of high emissive chiral bio-inorganic photonic films from the self-assembly of CdSe/CdS QRs. When the elastomeric film is stretched, the chiral nematic structure would reorientation into unidirectional nematic arrangement resulting the transformation of emission from circular polarization to linear polarization. Reproduced with permission from Ref. [61]. Copyright 2021, Wiley-VCH.

maximum g_{lum} could reach up to 0.45. The freestanding film of CNCs are usually rigid and fragile. To avoid this problem, Kang *et al.* firstly mix QRs with polyurethane [61]. After that, the mixture is added into CNCs suspension to fabricate freestanding films. The chiral elastomeric films with vivid structural color could stretch up to 120%. Besides, the films generate strong CPL with g_{lum} of 0.2. More intriguingly, dynamic change from linearly polarized emission to CPL can be observed when mechanical strain is applied to the film. The cholesteric helical structure would transform into unidirectional nematic organization leading to the changed polarization (Fig. 5d). This reversible structure could be further extended for fabricating novel functional and flexible photonic materials.

3.2. Template-free assembly of LDS

Apart from the template-assist assembly of LDS discussed above, LDS could self-assembly into highly ordered structure driving by the molecular or nanoscale interactions such as hydrogen bonding, C-H···π/π···π interaction, electrostatic interaction, van der Waals and metallophilic interactions between neighbored building blocks. In addition, directed self-assembly could also be realized by host-guest interactions and Langmuir-Schaeffer technique based on the interface interactions. The directed self-assembly provides a facile and universal strategy for obtaining chiral assembled structures. In this section, the state-of-art of template-free assembly of LDS will be introduced.

3.2.1. Self-assembly driving by nanoscale surface interactions

Non-covalent interactions which do not involve the sharing of electrons but relate to the dispersed vibration of electromagnetic interaction of molecules could play an important role in the self-assembly process of nanomaterials [62]. Driven by different non-covalent interactions such as hydrogen bonding, van der Waals, C-H···π/π···π, electrostatic interaction, and metallophilic interactions, individual NPs could self-assembly into an ordered structure.

Hydrogen bond is a strong non-covalent interaction which involves dipolar-dipolar attraction between a highly electronegative atom and a partially positive hydrogen atom. Feng's group report that achiral carbon QDs could be self-assembled into helical nanostructures in which the handedness of the nanowire is differentiated hydrogen bond in different solvents (Fig. 6a) [59]. First, achiral carbon QDs are synthesized by simple microwave method using conjugated Thioflavin (ThT) as a precursor. The obtained carbon QDs display astonishing quantum yield and are well dissolved in organic solvent. Surprisingly, when using H_2O as a poor solvent, the carbon QDs would form aggregate showing P-chirality with right-handed CPL response in ethanol-water bi-solvent system. However, the M-chirality self-assembly exhibiting left-handed CPL signal would appear in acetonitrile-water. The g_{lum} is in the range of 10^{-3}. Through a comprehensive study, the authors speculate the carbon QDs are initially aggregated and stacked layer by layer through π···π interaction to form nanowires. After that, left-handed helical nanostructures are formed in acetonitrile-water while P-chiral self-assembly is induced due to the enriched hydrogen bond in ethanol-water.

C-H···π interaction is a weak interaction between C-H bond and delocalized π electron. Similarly, the weak attraction between delocalized π electrons is known as π···π interaction. The C-H···π interaction plays a vital role during the self-assembly process and crystal packing of NPs. Wang *et al.* report Cu-based binuclear clusters could spontaneously assemble into layer structures

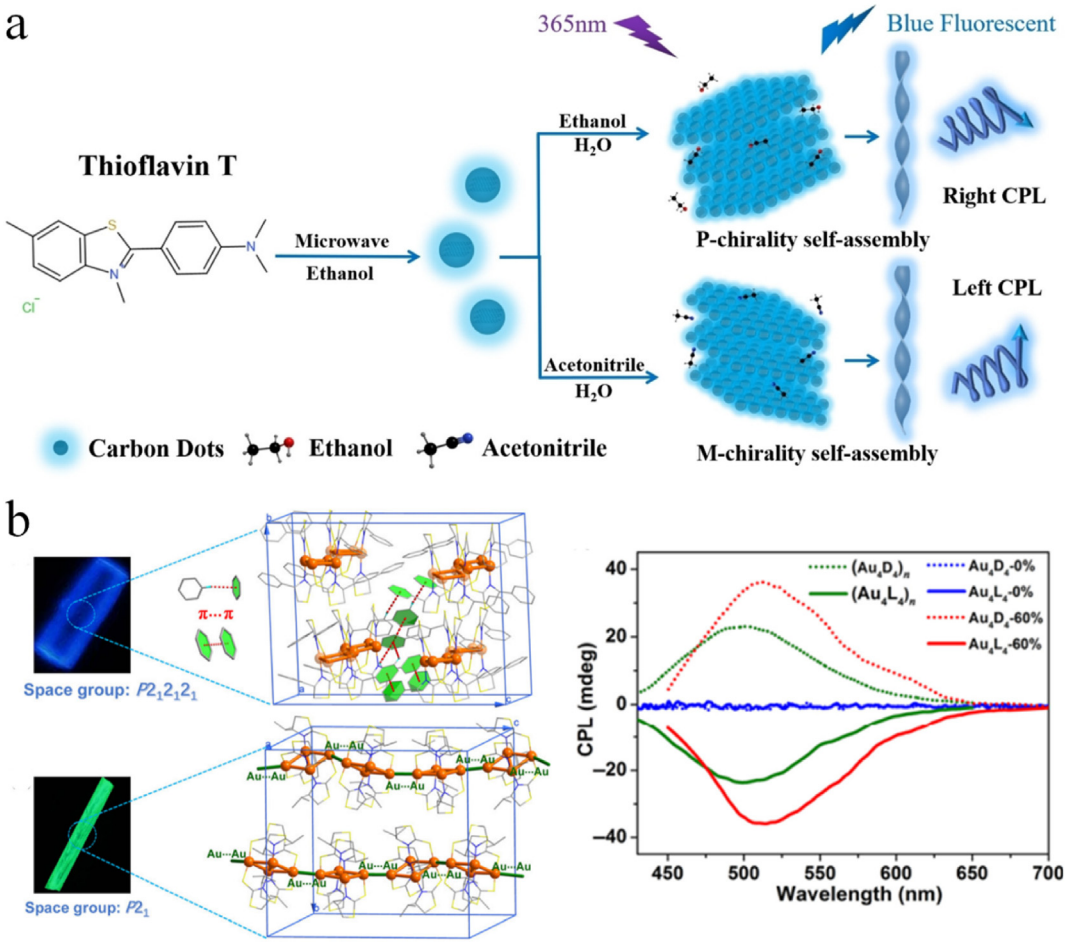

Fig. 6. (a) Illustration of the synthesis of achiral carbon dots from ThT and possible self-assembly mechanism. Bule fluorescent with opposite handedness could be observed excited at 365 nm. Reproduced with permission from Ref. [59]. Copyright 2022, Wiley-VCH. (b) Luminescent photograph of cluster and stacking structure of enantiomer for $(Au_4L_4)_n$ driven by intercluster Au-Au interactions. Right: CPL spectra of enantiomers of clusters dissolved in DMF with different amounts of water and solid state. Reproduced with permission from Ref. [68]. Copyright 2022, Springer Nature.

triggered by multiple C-H···π and C-H···C interaction [63]. (R/S)-2,2′-bis(diphenylphosphino)-1,1′-binaphthalene (R/R-BINAP) which have abundant naphthalene rings and benzene rings containing delocalized π electrons is chosen as the chiral organic phosphine ligands for synthesizing the cluster. When using the $Cu_2I_2(BINAP)_2$ clusters as building blocks, clusters could assemble into uniform hexagonal platelet-shaped microcrystals under the protection of polyvinyl-pyrrolidone micelles. The assembled microcrystals exhibit large g_{lum} of 9.5×10^{-3}. It is claimed that the intermolecular interactions among chiral ligands trigger the chiral stacking of clusters and effectively restrict the rotation of the benzene rings resulting a huge g_{lum} in the assembles. C-H···π interaction triggered self-assembly has also been witnessed in chiral Au clusters. As reported by Shi *et al.*, the Au cluster prepared in dichloromethane could assemble into body-centered cubic nanocubes *via* strong C-H···π interaction when adding *n*-hexane into the solution [64]. The CPL signal could also be enhanced in assembled superstructures due to the restricted movements of ligands.

Electrostatic interactions comprises strong attractions or repulsions between two oppositely charged units. During the formation of colloidal, ionic and other crystals, the electrostatic forces play a vital role. Recently, the electrostatic interactions could be applied at the nanoscale force to guide the assembly of LDS. Shi *et al.* realize the assembly of achiral Eu-containing polyoxometalates (POMs) with a diblock copolymer through electrostatic attraction [65]. The chirality transfer is realized in both ground and excited states from the polymer to the POM. In another example, Ji *et al.* achieve dimension-tunable CPL nanoassemblies. Cyanostilbene attached to a chiral glumatic acid by amidation (GluCN) is chosen as the building block [66]. The positively charged GluCN displays aggregation-induced emission (AIE) phenomenon in which the dimensional of the nanoassemblies could be regulated by the water content. Two achiral organic dyes (negatively charged CNA (a carboxylic cyanstibene) and positively charged ThT) are used to realize co-assemble with GluCN with different structures. When 3-dimensional nanocubes and 0-dimensional nanospheres of GluCN are assembled with ThT and CNA, neither the chirality transfer nor the energy transfer could be observed. When the positively charged ThT is used, one could observe energy transfer in which the emission peak shows a red shift. However, due to the electrostatic repulsion between the dye and GluCN, the ThT could only attach on the surface of the structure. Therefore, the energy transfer could be achieved while the chirality transfer is failed due to the spatial distance. As for the negatively charged CNA, both the energy transfer and chirality transfer could be realized. What is more, the g_{lum} is 1.0×10^{-2} of the co-assemblies when exciting using 340 nm irradiation which is 2.5 times bigger than the g_{lum} when directly exciting the CNA molecules. Electrostatic forces could also trigger acid-base interaction. Driven by acid-base interaction, Yuan *et al.* realize the co-assembly of helical tetraphenylethylene

(TPE) enantiomer with 4-dodecylbenzenesulfonic (DSA). The assembled superhelices display an enhanced CPL signal (more than 60-fold) compared with their molecular states. Moreover, the superhelices could further assemble with the addition of tartaric acid which show a g_{lum} up to 0.61 [67].

The weak interactions between the closed-shells (d^{10}, s^2) or pseudo-closed-shell d^8 of metal cations are considered as metallophilic interaction which could induce the assembly of NPs into superstructures. Transition metals such as Au, Ag and Cu exhibit metallophilic interactions that direct assemble into ordered structures. Zang's group achieve the assemble of chiral tetragold (I) clusters *via* inter-cluster Au-Au interaction which remarkably increases the quantum yield (Fig. 6b). The assemblies show a strong CPL signal with g_{lum} value of approximately 7.0×10^{-3} [68]. Apart from metallophilic interaction, the driving force for the assembly may have different origins. Yang *et al.* successfully obtains chiral assemblies Au (I) cluster with excitation wavelength-tunable CPL with g_{lum} approximately of 10^{-3} [69]. It is found that the synergetic mteallophilic interaction and Coulombic attraction direct the assemblies of the cluster giving rise to thermodynamically stable superstructures. Huang *et al.* report helical self-assemblies of Ag_{30} clusters driven by diverse non-covalent interaction [70]. They firstly synthesize racemic Ag_{30} clusters. It is found that the spontaneous self-resolution of the racemic clusters would occur through conglomerate crystallization in dimethylacetamide. The enantiomeric clusters in the racemic conglomerates are organized helically to form separate helical NP assemblies accompanied by CPL response with a g_{lum} of 7.0×10^{-4}. The helical assembly is driven by lots of weak interactions including B-H···π, C-H···π, π···π, and van der Waals force.

In short, the self-assembly on nanoarchitectures driven by non-covalent interactions is an efficient approach for constructing CPL-active materials. During the formation of assemblies, external stimuli, such as temperature, mechanical forces and pH, would influence the arrangements and morphologies of the products. Therefore, the CPL response might be regulated by external stimuli. Vortex flow has been recognized as an efficient non-chemical stimulus for supramolecular assembly. Numerous studies on vortex flow induced CPL have been reported in organic emitters [71,72]. Also, some other stimuli for regulating CPL have also been introduced in many excellent reviews [4,72,73].

3.2.2. LDS self-assembly driven by host-guest interaction

Host-guest interaction which involves two materials or molecules holding together in unique structural relationship by non-covalent bonding plays a vital role in the assembly of LDS. Generally speaking, a host contains a large cavity volume while the guest usually possesses complementary shape and interaction with the host which allows the enantioselective recognition between the host and guest [74]. Host-guest interaction-induced chirality transfer and amplification is an effective strategy to obtain self-assembly chiral LDS. By encapsulating achiral lanthanide complexes $La(acac)_3$ ($Ln = Eu_aTb_bGd_c$) into surface-coordinated chiral MOF, Zhai *et al.* successfully achieve CPL response of assembled lanthanide complexes (Fig. 7) [75]. To investigate the mechanism of induced CPL of the host-guest structure, powder of the composite material is mixed with the chiral MOF. The mixture displays strong CD signal and intensive emission while CPL signal is silent. Under this circumstance, the induced CPL could be ascribed to chirality transfer from the chiral host to the guest. Similarly, Zhang *et al.* realize the self-assembly of chiral MOF with perovskite nanocrystals. The encapsulated achiral perovskite could inherit chirality from the chiral MOFs by host-guest interaction in which the Eu and Pb atoms in the host could coordinate with the Br and O atoms in the perovskite, respectively [76]. The chirality could also be transferred from chiral guest to achiral host. Zhang's group successfully realizes CPL response from the guest-induced host-guest assembly in achiral MOF. Typically, enantiopure titanium-oxo clusters (R/S-TOCs) are used as chiral guests which have strong chirality, conjugated aggregation and chemical stability. The chiral clusters are positioned in the pores of the achiral MOF which display cyan emissions. The obtained R/S-TOC@NU-901 SURMOFs exhibit strong cyan emissions similar to the parent NU-901 SURMOFs. The g_{lum} could reach up to 0.025 which is much higher compared with traditional ligand induced chirality [77]. All these results prove that host-guest assembly could be an efficient strategy for chirality induction and amplification.

3.2.3. LDS self-assembly based on Langmuir-Schaeffer technique

Langmuir film is defined as an insoluble monolayer composed of molecules, atoms and NPs which is floated at the liquid-gas surface [78]. When Langmuir films are transferred from liquid-gas interface to solid support, Langmuir-Blodgett films are formed. Langmuir-Schaeffer is a variant of Langmuir-Blodgett deposition in which the deposition direction is horizontal. The Langmuir-Schaeffer technique is a promising method for preparing films with large scale and precise thickness. Recently, Langmuir-Schaeffer technique has been used for the solid state chiral assemblies of NPs [79]. Lv *et al.* firstly spread Au nanowire on the surface of a Langmuir trough. After that, aligned Au nanowires are obtained at the liquid-air surface by compressing the barrier. The aligned Au nanowires on the liquid-air surface are transferred to a quartz substrate by Langmuir-Schaeffer technique [80]. Then, a second layer could be deposited to construct chiral film by rotating the substrate at a certain angle. The as-prepared Langmuir-Schaeffer films display very strong CD response with several thousand mdegs across wide wavelength window ranging from NIR to visible region. This method has also been used to construct biomimetic chiral photonic films using $NiMoO_4{\cdot}xH_2O$ nanowires as building blocks. The as-prepared photonic films display strong circularly polarized color reflection observed in beetles [81]. Inspired by this work, the same group use $NiMoO_4{\cdot}xH_2O$ nanowires and CdSeS@ZnS core-shell QDs as building blocks to construct chiral photonic films with strong response based on Langmuir-Schaeffer technique (Fig. 8a) [82]. The photonic films have one dimensional helical structure similar to films obtained from the self-assembly of CNCs. Besides, the helical pitch of the films could be easily tuned by simply varying the rotation angle resulting a tunable PBG of films. The CPL response could be easily tuned by the helical pitch. By changing the emission wavelength of QDs, chiral photonic films with strong CPL response covering the whole visible range could be obtained. The maximum g_{lum} could reach up to 0.25.

Chen *et al.* successfully fabricate long-range ordered chiral CdSe/CdS nanorod film based on Langmuir-Schaeffer technique (Fig. 8b) [83]. Similar to the work of Lv *et al.*, CdSe/CdS nanorods floate disorderly at the liquid-air interface in Langmuir trough. By compressing the barrier, ordered alignment of nanorods are obtained. Then, the obtained Langmuir film is transferred from the liquid-air interface to a clean quartz. Chiral films are obtained by rotating the substrates clockwise or anticlockwise during the deposition process. The chiral films exhibit strong CPL signals with highest g_{lum} of 0.099 7. In addition, it is found that the number of layer and inter angel between two adjacent layers would influence the final CPL signal. Reports about usage of Langmuir-Schaeffer technique for constructing chiral NPs assemblies with CPL response are relative few. However, this technique exhibits enormous potential in constructing CPL-active nanomaterials with large g_{lum} and applications of CPL devices due to the precise control capability and low cost.

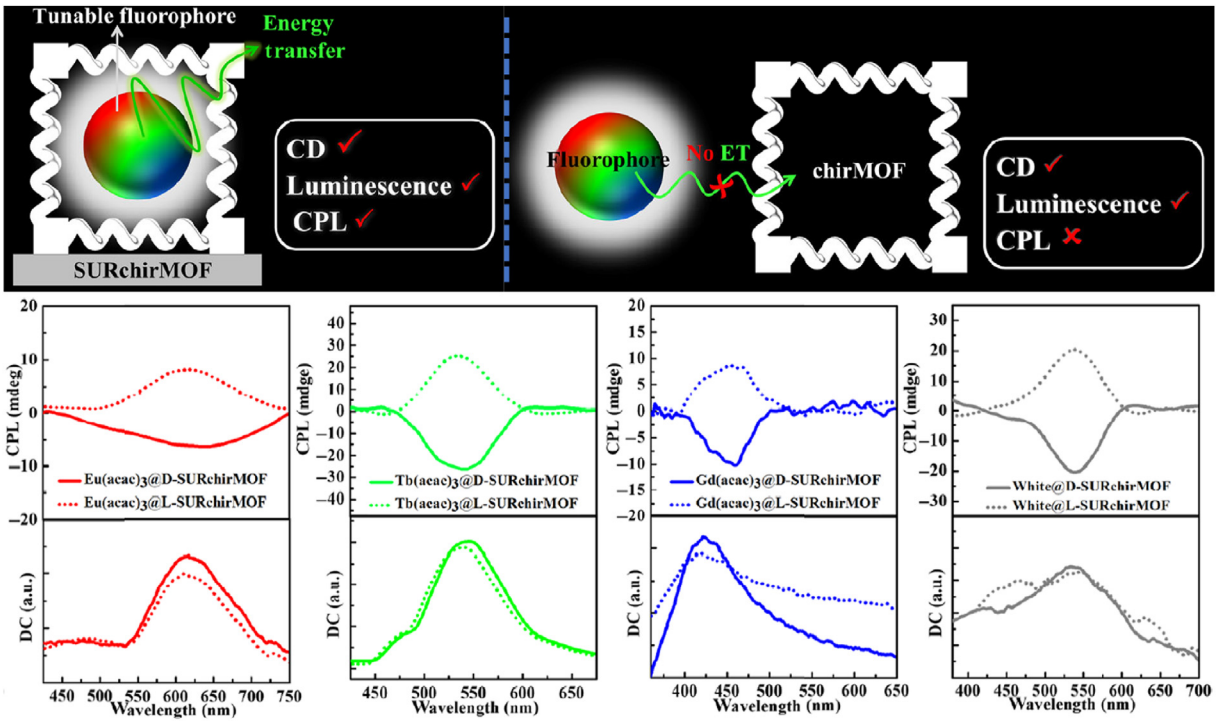

Fig. 7. Top: schematic representation of the energy transfer in the host-guest thin film of Ln(acac)$_3$@SURMOFs and no energy transfer in the mixture powder. Bottom: CPL spectra of different lanthanide complexes encapsulated in chiral MOFs. Reproduced with permission from Ref. [75]. Copyright 2021, Springer Nature.

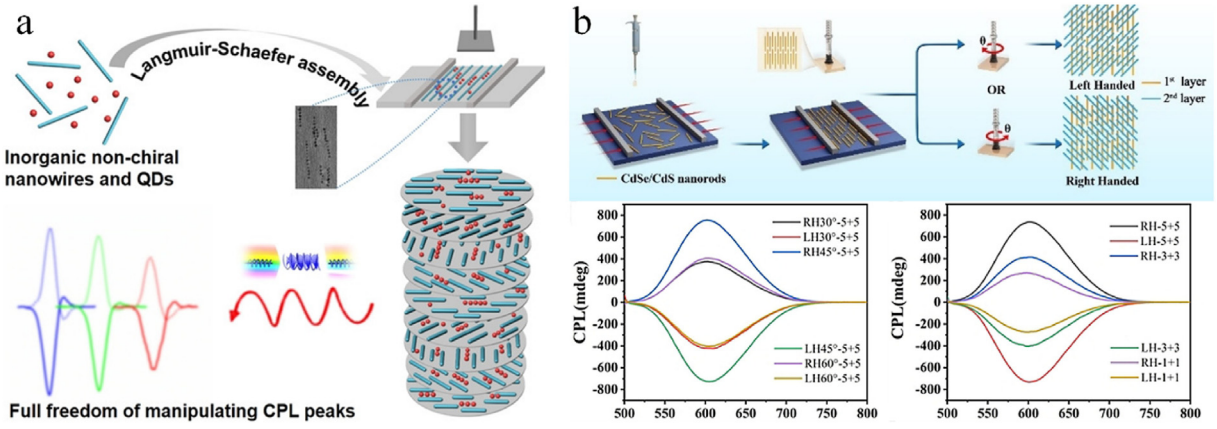

Fig. 8. (a) CdSSe@ZnS core–shell QDs are co-assembled with achiral nanowires to form chiral photonic crystals *via* Langmuir-Schaefer technique. The chiral photonic crystals display strong CPL response which could be easily manipulated by the emission wavelength of QDs. Reproduced with permission from Ref. [82]. Copyright 2022, Wiley-VCH. (b) Chiral films assemble from achiral CdSe/CdS nanorods by Langmuir-Schaeffer deposition. Reproduced with permission from Ref. [83]. Copyright 2021, Wiley-VCH.

4. Applications of self-assembled LDS associated CPL

Great efforts have been devoted to constructing CPL-active materials and enhancing the g_{lum}. CPL-active self-assembled LDS exhibit high quantum yield and g_{lum} that promise them excellent candidates for various applications. Here, some prominent applications such as circularly polarized light emitting diodes (CP-LEDs), optical information storage and encryption, CPL sensing and probing and enantioselective synthesis are highlighted.

4.1. CP-LED based on assembled LDS

Light emitting diodes (LEDs) are artificial light sources in which an emission layer sandwiched between anode and cathode. In LEDs display, high image contrast could be obtained by using a polarizer and a quarter wave plate to reduce the reflectivity from surroundings [1,84]. However, this method will cause a huge energy loss, resulting in reduced brightness, because only half of the light can reach the human eyes. CP-LEDs can overcome this drawback perfectly in which the energy loss originated from the polarizer and wave plate could be avoid [85]. Duan *et al.* report CP-LEDs using helical assembled chiral CdSe/CdS quantum dots-in-rods (CCCQs) as emitting layer with a turn-on voltage of 2.6 V which is comparable to commercial LEDs (Fig. 9a) [86]. Particularly, CCCQs are synthesized using chiral cholic acid as symmetry breaking agent. Right-handed helical structures are obtained from the side-by-side ranked CCCQs. The dissymmetry factor of circularly polarized electroluminescence (CPEL) is defined as $|g_{EL}| = |2(I_L - I_R)/(I_L + I_R)|$

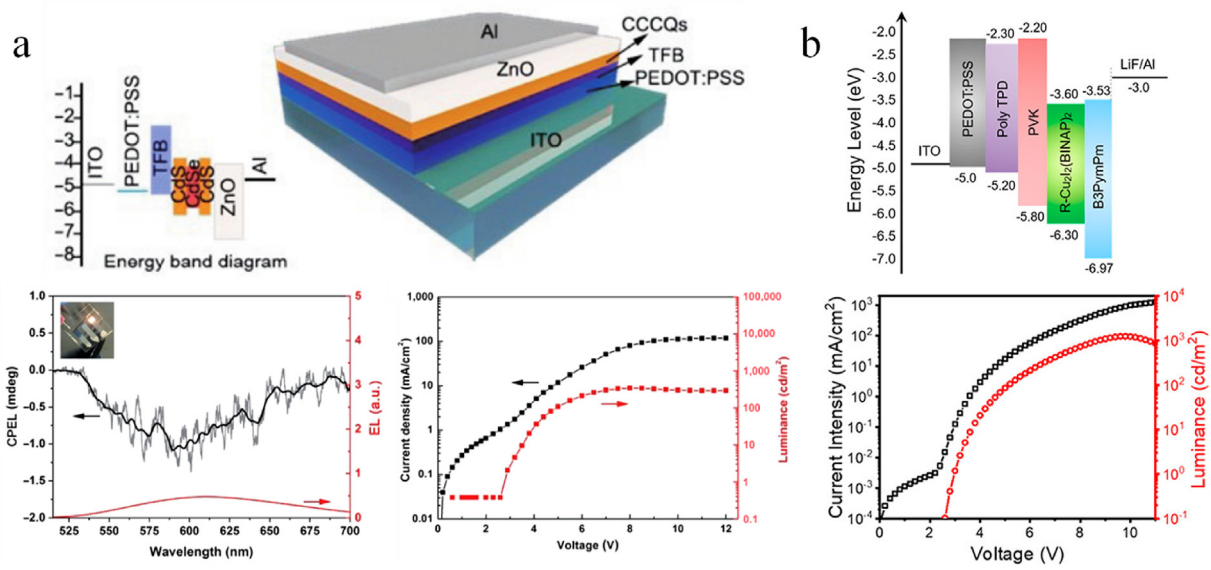

Fig. 9. (a) Top: energy level diagram of the electroluminescent device. Bottom: relationship between the current density, luminance and driving voltage. Reproduced with permission from Ref. [63]. Copyright 2021, American Chemical Society. (b) Energy level diagram of different functional layers and illustration of the structure of CP-LED. Bottom: CPL spectra and spectra of current density and luminance versus driving voltage for the electroluminescence device. Reproduced with permission from Ref. [86]. Copyright 2022, Springer Nature.

is 2×10^{-4}. The maximum external quantum efficiency (EQE) is 0.5% which is witnessed at a current density of 10 mA/cm^2 and a brightness at 135 cd/m^2. The relatively small g_{EL} and low EQE originated from various reasons. Chiral dislocation which is necessary for the CPEL in CCCQs would generate lots of electron and hole traps resulting in a low emitting efficiency. The g_{lum} is also very small resulting a small g_{EL}. Wang *et al.* successfully fabricate EL devices with a turn-on voltage of 2.9 V using solution processed $Cu_2I_2(BINAP)_2$ thin films as emitting layer (Fig. 9b) [63]. The EL device displays a high brightness of 1 200 cd/m^2 and a EQE of 0.54 %. The assembled copper cluster exhibits strong CPL signal with a broad emission peak in which the g_{lum} is 5×10^{-3} in oriented thin film. Nevertheless, the value of g_{EL} is not given.

In another example, Zang's group employs assembled Au cluster as emitting layer to fabricate CP-LEDs. The assembled Au clusters show PLQY of 41.4% and g_{lum} of 7×10^{-3} at aggregated state [68]. The home-made CP-LEDs have a turn-on voltage of 5 V. In addition, the CP-LEDs have a maximum EQE of 1.5%. The g_{lum} of -4.7×10^{-3} for S-LED and $+6.5 \times 10^{-3}$ for R-LED. It could deduce that the brightness and g_{lum} of CP-LED could be boosted *via* improving the PLQY and CPL response of nanomaterials. Besides, thermally activated delayed fluorescence (TADF) is an efficient method for improving the EQE of CP-LEDs since TADF materials can convert triplets to singlets through the reversed intersystem crossing process which could obtain 100 % internal quantum efficiency [87].

4.2. CPL sensing and probing based on self-assembled LDS

Comparing with other sensing techniques, fluorescence sensing has plenty of merits such as nondestructive, rapid and sensitive, in which analytes can interact with targets through molecular interactions or microenvironments changes [88]. CPL-active materials used for sensing could provide higher sensitivity and resolution since it could eliminate the interference of unpolarized light and the background emission [4,89]. As mentioned previously, Suo *et al.* realize chiral assembly of AuAg bimetallic nanoclusters using G-quartet nanofiber. The assembled chiral structure display strong CPL response [43]. Based on the interaction between the nanoclusters and thiol group, the right-handed helical nanofibers are used as biosensor to detect Cys molecules which is an amino acid highly associated with certain diseases. With the increase of Cys molecules concentration, CPL signals of the assembled structures exhibit a decreased tendency. The limit of detection of the proposed system for Cys molecules is estimated to be 95.7 nM. In addition, the proposed sensing system exhibits very high selectivity for Cys molecules comparing with other essential amino acids under identical condition (Fig. 10a).

When some microenvironments change, fluorescent may not be affected, but CPL is sensitive to these changes, and thus CPL can be used as indicator to detect the changes. Liu's group demonstrates tunable UC-CPL emission by the co-assembly of CNCs and UCNPs [90]. The PBGs of the photonic films could be precisely controlled by the addition of glycerol which results in a tunable CPL emission from blue to red. It is found that the obtained glycerol-composite photonic film is sensitive to humidity. When the relative humidity (RH) decreases from 85% to 33%, the CPL signals increase significantly. The value of $|g_{lum}|$ increases from 0.033 to 0.156 with the decrease of RH. However, the DC spectra are almost unchanged, indicating that the emission from UCNPs is not affected when PBGs blue shifts from 581 to 505 nm. The increased g_{lum} could be originated from the increased overlap between the emission band of UNCPs and the blue shifted PBGs of photonic films with decreasing RH (Fig. 10b).

Chiral molecules are stereoselective, in which enantiomers exhibit significant differences in their physiological reactions in organism [91]. For instance, R-enantiomer of thalidomide could be used as medicine with desirable sedative effect while the L-enantiomer would cause serious embryo-toxic and teratogenic effect [92]. Therefore, it is important to recognize the molecular chirality of enantiomers. CPL probe could be a powerful technique to distinguish enantiomers. Achiral zeolitic imidazolate framework (ZIF-8) could be used as template to realize the assembly of chiral binaphthyl-derived emitters that enhance CPL [93]. The g_{lum} could be significantly increased from 10^{-4} to 10^{-3} owing to the ordered arrangement of the chiral emitter. Besides, the fluorescence efficiency could also be improved. The chiral emitter possesses chiral

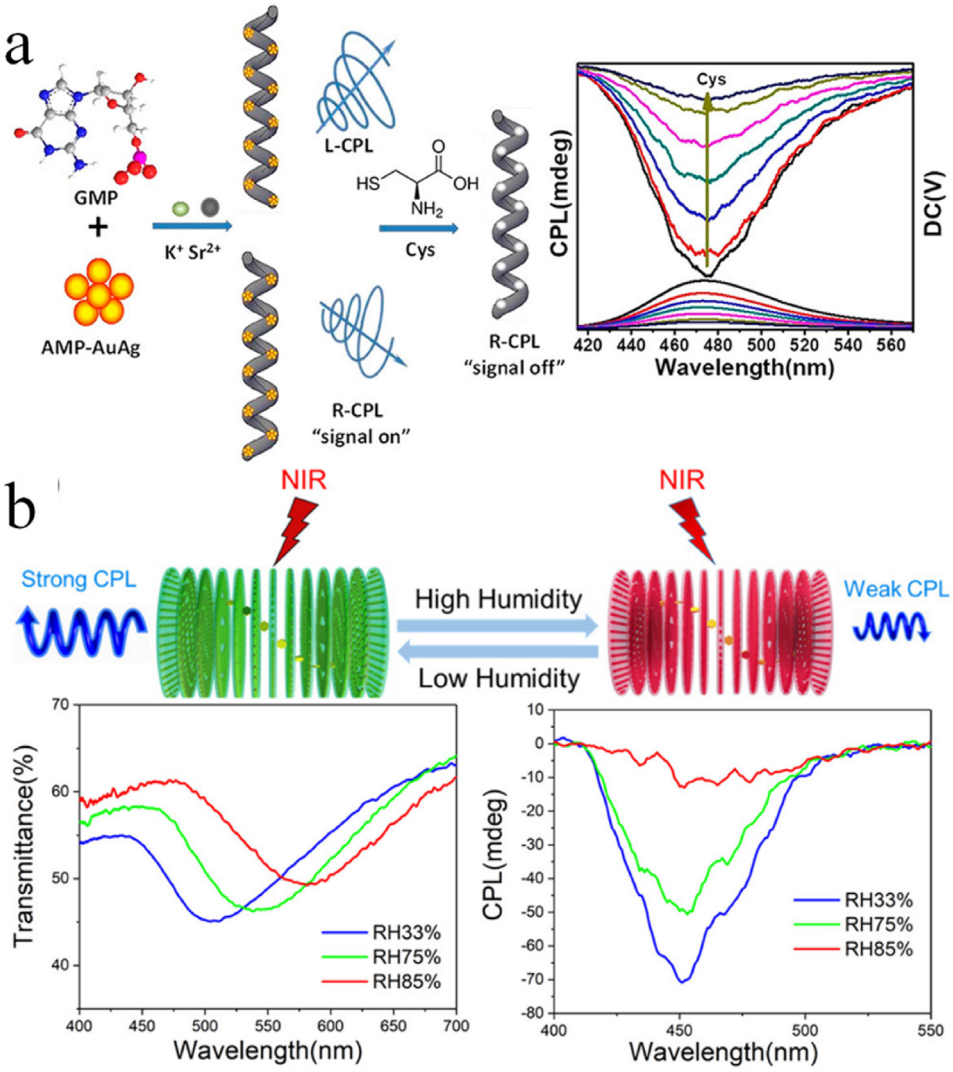

Fig. 10. (a) Schematic of the humidity response of UC-CPL by chiral photonic films. Transmission and CPL spectra of chiral photonic films at different RH. Reproduced with permission from Ref. [90]. Copyright 2019, American Chemical Society. (b) Illustration of the assembly of GMP and bimetallic cluster and CPL response with different amount of Cys. Reproduced with permission from Ref. [43]. Copyright 2020, American Chemical Society.

binaphthyl and -NH- groups which might be used for the enantioselective recognition of α-hydroxycarboxylic acids. Triggered by an intramolecular photoinduced electron transfer (PET) process, the long pair electrons in the nitrogen atom could quench the fluorescence of the emitter while mixing with α-hydroxycarboxylic acid could block the PET process leading a fluorescence enhancement. Comparing with L-tartaric acid, the fluorescence of R-ZIF mixed with D-tartaric acid displays a faster enhancement. A higher enantioselectivity could be observed for mandelic acid. This work provides a simple approach for enantioselective recognition.

4.3. Optical information storage and encryption

Information recording and encryption play a dramatic role in our daily life. Photo-responsive materials could be used for storing and delivering information [94]. Comparing to traditional photo-responsive materials, CPL-active materials could achieve higher storage density and security in which the emission and the chiral response could be used simultaneously [4]. By doping green emission QDs into CNCs, Xu *et al.* construct CPL photonic films for optical coding with quick response (Fig. 11a) [95]. Typically, the code disappears observing with a left-handed circularly polarized filter (L-CPF) under natural light. The code pattern could be clearly observed when using a right-handed circularly polarized filter (R-CPF) which indicates the transmission of R-CPL and selective reflection of L-CPL of the photonic films. In addition, the code could be easily observed through R-CPF comparing with L-CPF under UV irradiation in which the emission intensity is larger in the R-CPF cases because the optical label displays strong R-CPL response.

Dynamic control CPL and photoluminescence of materials would make them attractive for optical storage devices. Guo's group fabricates rewritable optical storage devices based on self-organized emissive superstructures in which chiral fluorescent dye named as photo-switch 6 and UCNPs are doped in nematic liquid crystals simultaneously [96]. The reversible CPL could be triggered by the power density of a 980 nm laser. When the laser power is low, green emission centered at 520 nm is dominated corresponding to the energy transfer between Yb^{3+} and Er^{3+} which is overlapped with the absorption band of a trans form of switch 6. The 365 nm UV and 450 nm blue emissions consisting to the energy transfer between Yb^{3+} and Tm^{3+} could be obtained when the excitation power is high. The green emission would trigger the

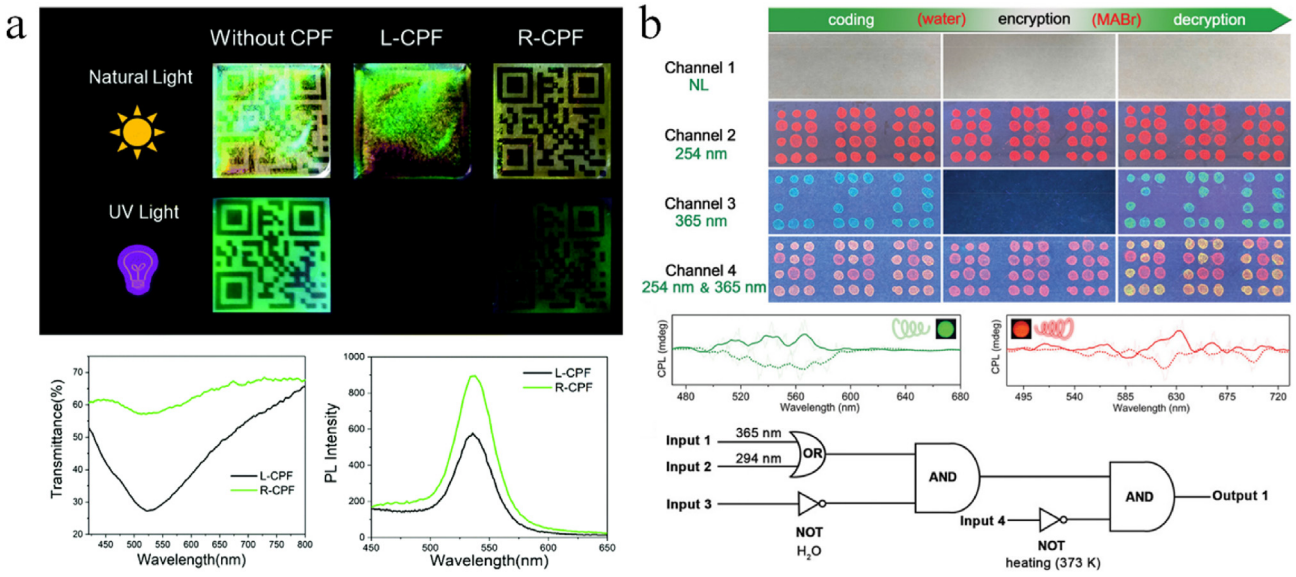

Fig. 11. (a) Photograph of code covered with chiral photonic films taken with or without CPF. Bottom: transmission and PL spectra of chiral photonic films under CPF. Reproduced with permission from Ref. [95]. Copyright 2019, The Royal Society of Chemistry. (b) Reversible CPL and PK switching of ZZU pattern on the filter paper in one information coding-encryption-decryption cycle. Middle: CPL spectra of the assembled structures under different excitation. Bottom: schematic of the integrated chiral logic gate. Reproduced with permission from Ref. [76]. Copyright 2022, Wiley-VCH.

photoisomerization of switch 6 from a trans to cis state while the reverse isomerization could be realized by the UV and blue emission. Besides, the CPL signal and g_{lum} could also be dynamically controlled by the power density of laser. Based on this, a PL/CPL-encryption dual-mode optical storage device can be designed. By using a photomask, fluorescent dot array could be written on cell with a high-power laser. In addition, the information could be easily erased at low power density.

In another example, achiral $MAPbBr_3$ perovskite NPs and chiral MOF are co-assembled (Fig. 11b) [76]. The perovskite could inherent the chirality of MOF by coordination bonds. The CPL could be regulated by various external stimuli. When adding water into the assembled structure, CPL will be quenched due to the decomposition of $MAPbBr_3$. The dismissed CPL signal can be recovered by adding MABr ethanol solvent. Moreover, switched CPL response could also be obtained by changing temperature. The assembly structures show a gradual decrease of CPL with the increase of temperature from 293 to 333 K, and completely vanish at 373 K. The CPL signal can recover after cooling down to 293 K. Moreover, reversible CPL could be realized between the green emission of perovskite and the red emission of chiral MOF by varying excitation wavelength. A chiroptical logic gate is fabricated in which these stimuli are used as inputs, CPL signals are used as outputs. The obtained chiral logic gate will be used for multiple information encryption and decryption. These multiple external stimuli increase the optical storage density and improve the security of information.

4.4. Enantioselective synthesis

Enantioselective synthesis refers to the preparation of compounds guiding the synthesis in the favor of producing one stereoisomer over another. CPL has been applied for inducing the asymmetric photochemical synthesis which is a vital type of enantioselective synthesis [97]. CPL-active materials are potential light sources for triggering enantioselective synthesis. We have fabricated chiral photonic films *via* the co-assembly of blue emissive Si QDs and CNCs (Fig. 12) [56]. The obtained photonic films show extensive R-CPL with high g_{lum}. 10,12-Tricosadiynoic acid (DA) molecules could be polymerized into polydiacetylene (PDA) chain under the irradiation of light. The initiation process of DA molecules could be activated by UV light while chiral structures could be induced by CPL during the chain propagation process [98]. In this way, the photonic film excited by a 355 nm laser and a UV lamp where the central wavelength of 254 nm are used for preparing PDA (Fig. 12b). The prepared PDA film shows negative CD signal in the spectrum. However, restricted by the native left-handed structure of the photonic film, chiral PDA with another handedness could not be fabricated by this approach. Jin *et al.* prepare helical nanotubes with UC-CPL by the co-assembly of chiral lipid gelator and achiral lanthanide-doped UCNPs [49]. The UV region of UC-CPL from the nanotube could trigger the polymerization of 2,4-heneicosadiynoic acid into PDA chain. Interestingly, the handedness of PDA chain could be precisely controlled by the helical nanotube. Negative CD signals are observed when D-GAm/UCNPs nanotube is used as light source while positive signals are witnessed in L-GAm/UCNPs system. These works emphasize the enormous potentials of employing CPL-active materials as light source for asymmetry synthesis.

4.5. Bioimaging

Developing precise imaging techniques for monitoring and analyzing biological species is urgent. Comparing with traditional fluorescence contrast probes which suffers low-precision and low-resolution imaging, CPL-active emitters could have higher storage density in which both the emission intensity and chiral behavior could be applied for probe. What is more, chirality is strongly related to the fundamentals of life. CPL spectroscopy enables us to study the chiral interaction between the probes and their binding motifs in cells. Zang's group develops a pair of enantiomeric copper(I) alkynyl clusters (R/S-Cu_{14}) which display PL and CPL response simultaneously triggered by unique AIE and crystallization-induced emission effects [99]. In cell medium, the PL of the clusters could be stable over 1 day. The standard Cell Counting Kit 8 (CCK-8) assay test shows the cytotoxicity of R-Cu_{14} cluster is smaller than the

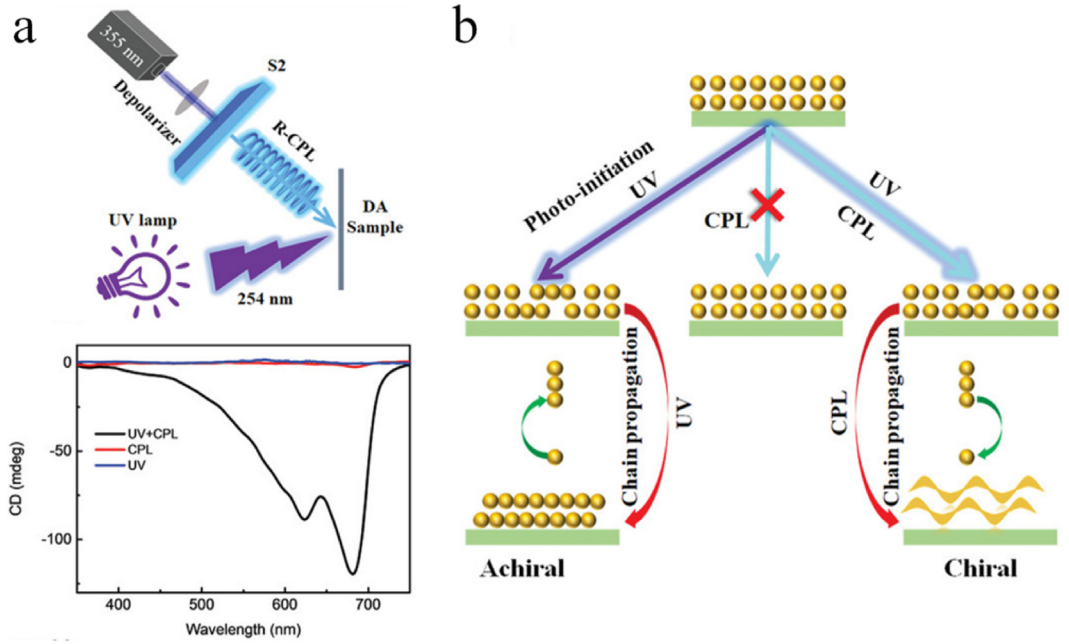

Fig. 12. (a) Top:Experimental setup for the preparation of photopolymerization of DA molecules; Bottom: CPL spectra of prepared films under different illumination. (b) possible mechanism for the photopolymerization process. Reproduced with permission from Ref. [56]. Copyright 2022, Wiley-VCH.

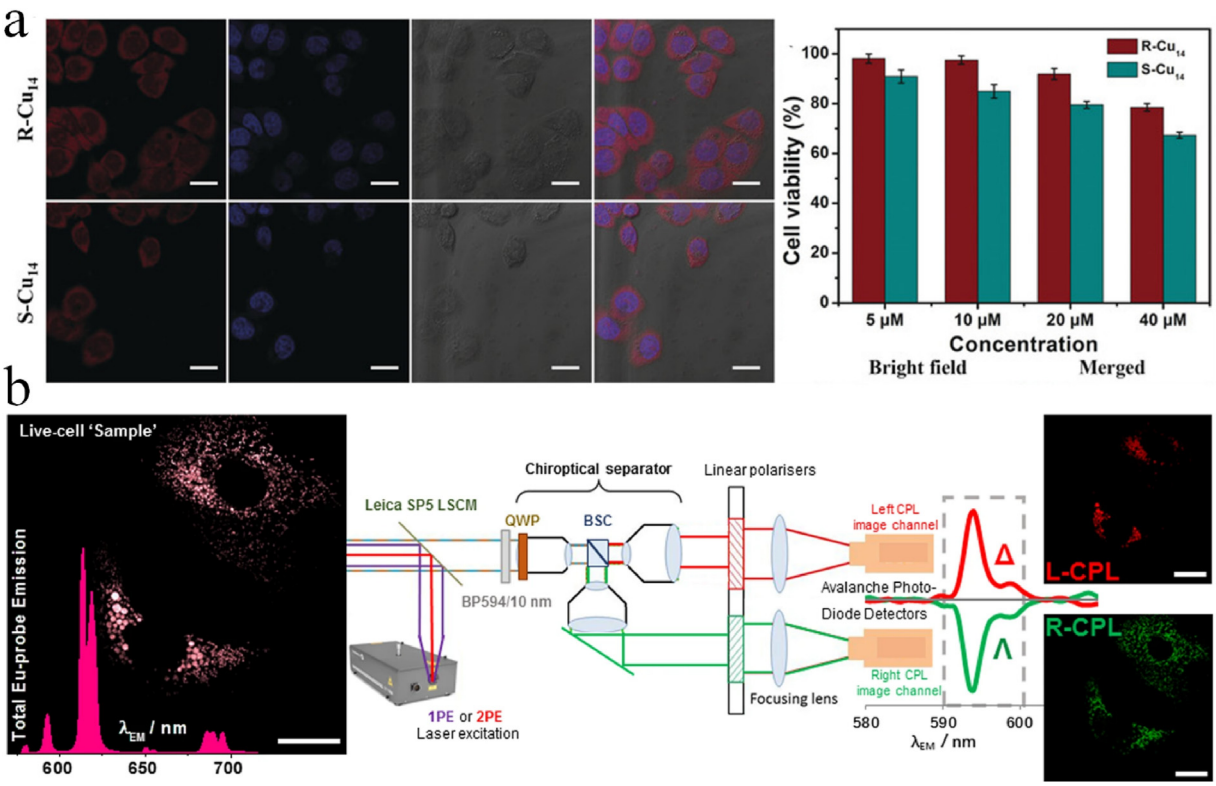

Fig. 13. (a) Confocal image of HeLa cells incubated with clusters for 24 h and viability of HeLa cells. Reproduced with permission from Ref. [99]. Copyright 2020, Wiley-VCH. (b) Experiment setup of the CPL laser scanning confocal microscope and the diffraction-limited enantioselective image of the CPL-active probes with live cells. Reproduced with permission from Ref. [101]. Copyright 2022, Springer Nature.

other one which could be attributed to a stereospecific interaction between the cluster and cells. Moreover, by treated HeLa cells and NG108-15 cells with 5 μM clusters in cell medium, live cell imaging could be realized. All these results indicates that the CPL-active clusters could be a promising probe for bioimaging (Fig. 13). In another example, Frawley and colleagues employ bright Eu complex as CPL emitter for realizing the chiral image contrast [100]. The proof-of-concept of chiral imaging could improve the quality and

contrast of image. In their following work, they extend the CPL measurement technology to CPL laser scanning confocal microscopy [101]. The proposed method could gather L-CPL and R-CPL images for enantioselective differential contrast microscopy with a small spatial resolution. The proposed approach has been successfully applied for the imaging of live NIH 3T3 cells.

5. Conclusion and perspectives

CPL-active nanomaterials have aroused enormous interests and been experienced rapid growth. The introduction of "self-assembly" makes the construction more convenient and efficient. The assembled structures could not only induce chirality of nanomaterials but also significantly increase the g_{lum} compared with their individual state. Here, recent progresses in assembled CPL-active nanomaterials have been highlighted. Self-assembly of LDS with strong CPL response could be guided by various chiral templates such as DNA-base soft templates, CNCs and chiral gelators. Driven by various non-covalent interaction such as hydrogen bonding, van der Waals interaction and metallophilic interaction, individual unit could self-assembly into chiral nanostructures without the assistance of templates. In addition, the assembled structures with CPL response are useful for various applications in CP-LEDs, CPL sensing and probing, optical information process and enantioselective synthesis.

Although significant achievements have been realized, the development of CPL from LDS based on self-assembled chiral structures is still in its early stages. In this rapidly growing research field, there are still many challenges to be addressed. First of all, the constructions of CPL-active assembled structures are well presented in many publications while the underlying mechanisms are not well explained. Usually, the CPL activity are simply explained by the chirality transfer or induction mechanisms proposed for CD behavior since CPL could be regarded as an analogy of CD. However, the CPL is more complex because it is related to the excited state information and configuration, while CD is only related to the ground state. In some cases, these two processes belong to different transitions. Simulation methods and theories to address the luminescence of chiral assembled structures are also insufficient.

Secondly, it is known that ideal CPL emitters should have high quantum yield and large g_{lum} simultaneously. As mentioned previously, a high quantum yield usually requires a large electric transition dipole moment. However, a small g_{lum} would be obtained when the electric transition dipole moment is large if there is no other photophysical mechanism. More efforts need to be devoted to breaking the trade-off effect. Besides, when constructing self-assembly structures, it is usually suffering aggregation-caused quenching resulting in low emission efficiency. Only when CPL-active assembled structures have significantly large g_{lum} and quantum efficiency, their performance can be maximized in various applications.

Thirdly, commercial CPL spectrometers can only cover short wavelength region, which severely restricts the development of CPL-active materials in NIR and microwave regions. By constructing chiral UNCPs, NIR excitation could be realized by changing light source, and some groups have reported the results. However, this instrument modifications are time-consuming and not kind to researchers who are not familiar with photophysics. Besides, CPL of LDS in NIR region is rarely reported due to the lack of commercial detection instruments of the circularly polarized emission signal. As a result, developing CPL instrument with excitation and detection at long wavelength is needed. In addition, extending CPL wavelength to NIR or even longer region would not only deepen our understanding of the underlying mechanism for CPL-active materials, but also trigger tremendous optoelectronic and biological applications.

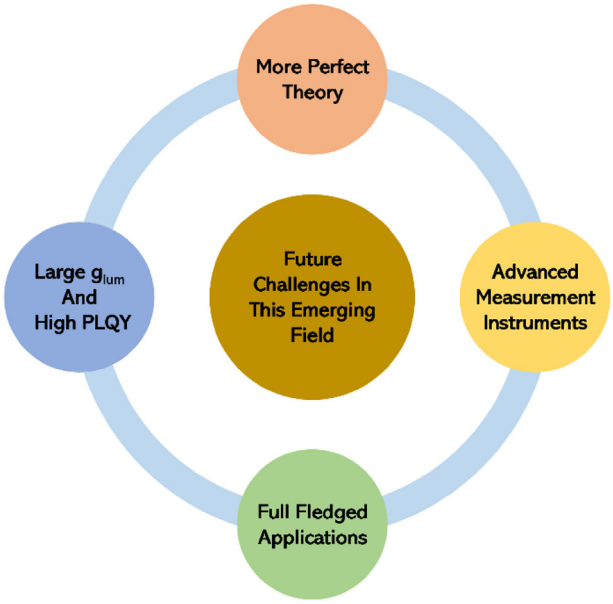

Fig. 14. Summary of future challenges in this field.

Finally, applications based on CPL-active assembled structures are inspirational and develop rapidly with huge potential in many emerging areas. However, the applications are still infancy, and further efforts should be devoted (Fig. 14). Overall, this review is expected to provide inspiration for the audiences and enrich the research area of CPL-active assembled structures from low dimensional nanomaterials, driving further development of advanced chiroptical science.

Declaration of competing interest

The authors declare that they have no known competing financial interests or personal relationships that could have appeared to influence the work reported in this paper.

Acknowledgements

This work is supported by the National Natural Science Foundation of China (62174079), Science, Technology and Innovation Commission of Shenzhen Municipality (Projects Nos. JCYJ20220530113015035, JCYJ20210324120204011 and KQTD2015071710313656). The authors would like to thank Dr. Jiaji Cheng for fruitful discussions.

References

[1] Sang YT, Han JL, Zhao TH, Duan PF, Liu MH. Circularly polarized luminescence in nanoassemblies: generation, amplification, and application. Adv Mater 2020;32:1900110.
[2] Zhang YD, Yu S, Han B, Zhou YL, Zhang XW, Gao XQ, Tang ZY. Review Circularly polarized luminescence in chiral materials. Matter 2022;5:837–75.
[3] MacKenzie LE, Pal R. Circularly polarized lanthanide luminescence for advanced security inks. Nat Rev Chem 2021;5:109–24.
[4] Deng YJ, Wang MZ, Zhuang YL, Liu SJ, Huang W, Zhao Q. Circularly polarized luminescence from organic micro-/nano-structures. Light Sci Appl 2021;10:76.
[5] Zhou L, Ni F, Li N, Wang K, Xie GH, Yang CL. Tetracoordinate boron-based multifunctional chiral thermally activated delayed fluorescence emitters. Angew Chem Int Ed 2022;61:e202203844.
[6] Jiang S, Kotov NA. Circular polarized light emission in chiral inorganic nanomaterials. Adv Mater 2022:2108431.
[7] Wang J, Fang C, Ma JQ, Wang S, Jin L, Li WC, Li DH. Aqueous synthesis of low-

dimensional lead halide perovskites for room-temperature circularly polarized light emission and detection. ACS Nano 2019;13:9473–81.
[8] Hananel U, Ben-Moshe A, Tal D, Markovich G. Enantiomeric control of intrinsically chiral nanocrystals. Adv Mater 2020;32:1905594.
[9] Gao XQ, Han B, Yang XK, Tang ZY. Perspective of chiral colloidal semiconductor nanocrystals: opportunity and challenge. J Am Chem Soc 2019;141:13700–7.
[10] Lv JW, Gao XQ, Han B, Zhu YF, Hou K, Tang ZY. Self-assembled inorganic chiral superstructures. Nat Rev Chem 2022;6:125–45.
[11] Zhang X, Xu YY, Valenzuela C, Zhang XF, Wang L, Feng W, Li Q. Liquid crystal-templated chiral nanomaterials: from chiral plasmonics to circularly polarized luminescence. Light Sci Appl 2022;11.
[12] Zhang C, Li S, Dong XY, Zang SQ. Circularly polarized luminescence of agglomerate emitters. Aggregate 2021;2:e48.
[13] Chen WJ, Ma K, Duan PF, Ouyang GH, Zhu XF, Zhang L, Liu MH. Circularly polarized luminescence of nanoassembliesviamulti-dimensional chiral architecture control. Nanoscale 2020;12:19497–515.
[14] Tanaka H, Inoue Y, Mori T. Circularly polarized luminescence and circular dichroisms in small organic molecules: correlation between excitation and emission dissymmetry factors. Chemphotochem 2018;2:386–402.
[15] Riehl JP, Richardson FS. Circularly polarized luminescence spectroscopy. Chem Rev 1986;86:1–16.
[16] Richardson FS, Riehl JP. Circularly polarized luminescence spectroscopy. Chem Rev 1977;77:773–92.
[17] Arrico L, Di Bari L, Zinna F. Quantifying the overall efficiency of circularly polarized emitters. Chem Eur J 2021;27:2920–34.
[18] Nagata Y, Mori T. Irreverent nature of dissymmetry factor and quantum yield in circularly polarized luminescence of small organic molecules. Front Chem 2020;8:00448.
[19] Yao L, Niu GD, Li JZ, Gao L, Luo XF, Xia B, Liu YH, Du PP, Li DH, Chen C, Zheng YX, Xiao ZW, Tang J. Circularly polarized luminescence from chiral tetranuclear copper(I) iodide clusters. J Phys Chem Lett 2020;11:1255–60.
[20] Wong KL, Bunzli JCG, Tanner PA. Quantum yield and brightness. J Lumin 2020;224:1.
[21] Samoilov BN. Luminescence from a chiral crystal of sodium uranyl acetate. J Exp Theor Phys 1948;18:1030–40.
[22] Longhi G, Castiglioni E, Koshoubu J, Mazzeo G, Abbate S. Circularly polarized luminescence: a review of experimental and theoretical aspects. Chirality 2016;28:696–707.
[23] Shindo Y, Nakagawa M. On the artifacts in circularly polarized emission spectroscopy. Appl Spectrosc 1985;39:32–8.
[24] Kondo Y, Suzuki S, Watanabe M, Kaneta A, Albertini P, Nagamori K. Temperature-Dependent circularly polarized luminescence measurement using KBr pellet method. Front Chem 2020;8:00527.
[25] Steinberg IZ, Gafni A. Sensitive instrument for the study of circular polarization of luminescence. Rev Sci Instrum 1972;43:409–13.
[26] Tinoco I, Ehrenberg B, Steinberg IZ. Fluorescence detected circular dichroism and circular polarization of luminescence in rigid media: direction dependent optical activity obtained by photoselection. J Chem Phys 1977;66:916–20.
[27] Harada T, Kuroda R, Moriyama H. Solid-state circularly polarized luminescence measurements: theoretical analysis. Chem Phys Lett 2012;530:126–31.
[28] Meskers SCJ, Peeters E, Langeveld-Voss BMW, Janssen RAJ. Circular polarization of the fluorescence from films of poly(p-phenylene vinylene) and polythiophene with chiral side chains. Adv Mater 2000;12:589–94.
[29] Castiglioni E, Abbate S, Lebon F, Longhi G. Ultraviolet, circular dichroism, fluorescence, and circularly polarized luminescence spectra of regioregular poly-[3-((S)-2-Methylbutyl)-Thiophene] in solution. Chirality 2012;24:725–30.
[30] Urry DW, Krivacic J. Differential scatter of left and right circularlay polarized light by optically active particulate systems. Proc Natl Acad Sci USA 1970;65:845–52.
[31] Wan L, Wade J, Salerno F, Arteaga O, Laidlaw B, Wang X, Penfold T, Fuchter MJ, Campbell AJ. Inverting the handedness of circularly polarized luminescence from light-emitting polymers using film thickness. ACS Nano 2019;13:8099–105.
[32] Kim YJ, Li HC, He Y, Chen X, Ma XT, Lee M. Collective helicity switching of a DNA-coat assembly. Nat Nanotechnol 2017;12:551–6.
[33] Kneer LM, Roller EM, Besteiro LV, Schreiber R, Govorov AO, Liedl T. Circular dichroism of chiral molecules in DNA-assembled plasmonic hotspots. ACS Nano 2018;12:9110–5.
[34] Yan WJ, Xu LG, Xu CL, Ma W, Kuang H, Wang LB, Kotov NA. Self-assembly of chiral nanoparticle pyramids with strong R/S optical activity. J Am Chem Soc 2012;134:15114–21.
[35] Kuzyk A, Schreiber R, Fan ZY, Pardatscher G, Roller EM, Hogele A, Simmel FC, Govorov AO, Liedl T. DNA-based self-assembly of chiral plasmonic nanostructures with tailored optical response. Nature 2012;483:311–4.
[36] Gorecki M, Zinna F, Biver T, Di Bari L. Induced circularly polarized luminescence for revealing DNA binding with fluorescent dyes. J Pharm Biomed Anal 2017;144:6–11.
[37] Jiang Q, Xu XH, Yin PA, Ma K, Zhen YG, Duan PF, Peng Q, Chen WQ, Ding BQ. Circularly polarized luminescence of achiral cyanine molecules assembled on DNA templates. J Am Chem Soc 2019;141:9490–4.
[38] Chen JQ, Chen YY, Zhao LJ, Feng LY, Xing FF, Zhao CQ, Hu LZ, Ren JS, Qu XG. G-quadruplex DNA regulates invertible circularly polarized luminescence. J Mater Chem C 2019;7:13947–52.
[39] Chen JQ, Liu XW, Suo ZG, Gao CQ, Xing FF, Feng LY, Zhao CQ, Hu LZ, Ren JS, Qu XG. Right-/left-handed helical G-quartet nanostructures with full-color and energy transfer circularly polarized luminescence. Chem Commun 2020;56:7706–9.
[40] Carvalho J, Mergny JL, Salgado GF, Queiroz JA, Cruz C. G-Quadruplex, friend or foe: the role of the G-quartet in anticancer strategies. Trends Mol Med 2020;26:848–61.
[41] Martin-Arroyo M, del Prado A, Chamorro R, Bilbao N, Gonzalez-Rodriguez D. Elucidating noncovalent reaction mechanisms: G-quartet as an intermediate in G-quadruplex assembly. Angew Chem Int Ed 2020;59:9041–6.
[42] Stefan L, Monchaud D. Applications of guanine quartets in nanotechnology and chemical biology. Nat Rev Chem 2019;3:650–68.
[43] Suo Z, Hou X, Chen J, Liu X, Liu Y, Xing F, Chen Y, Feng L. Highly chiroptical detection with gold–silver bimetallic nanoclusters circularly polarized luminescence based on G-quartet nanofiber self-assembly. J Phys Chem C 2020;124:21094–102.
[44] Yu XD, Chen LM, Zhang MM, Yi T. Low-molecular-mass gels responding to ultrasound and mechanical stress: towards self-healing materials. Chem Soc Rev 2014;43:5346–71.
[45] Williams GT, Haynes CJE, Fares M, Caltagirone C, Hiscock JR, Gale PA. Advances in applied supramolecular technologies. Chem Soc Rev 2021;50:2737–63.
[46] Hao CL, Gao YF, Wu D, Li S, Xu LG, Wu XL, Guo J, Sun MZ, Li X, Xu CL, Kuang H. Tailoring chiroptical activity of iron disulfide quantum dot hydrogels with circularly polarized light. Adv Mater 2019;31:1903200.
[47] Liu CC, Yang JC, Lam JWY, Feng HT, Tang BZ. Chiral assembly of organic luminogens with aggregation-induced emission. Chem Sci 2022;13:611–32.
[48] Shi YH, Duan PF, Huo SW, Li YG, Liu MH. Endowing perovskite nanocrystals with circularly polarized luminescence. Adv Mater 2018;30:1705011.
[49] Jin X, Sang YT, Shi YH, Li YG, Zhu XF, Duan PF, Liu MH. Optically active upconverting nanoparticles with induced circularly polarized luminescence and enantioselectively triggered photopolymerization. ACS Nano 2019;13:2804–11.
[50] Cao R, Yang XK, Wang Y, Xiao Y. Induced circularly polarized luminescence of perovskite nanocrystals by self-assembly chiral gel. Nano Res 2023;16:1459–64.
[51] Xie HX, Du HS, Yang XG, Si CL. Recent strategies in preparation of cellulose nanocrystals and cellulose nanofibrils derived from raw cellulose materials. Int. J. Polym. Sci. 2018;2018:7923068.
[52] Shi Y, Zhou ZM, Miao XF, Liu YJ, Fan QL, Wang K, Luo D, Sun XW. Circularly polarized luminescence from semiconductor quantum rods templated by self-assembled cellulose nanocrystals. J Mater Chem C 2020;8:1048–53.
[53] Zheng HZ, Ju B, Wang XJ, Wang WH, Li MJ, Tang ZY, Zhang SXA, Xu Y. Circularly polarized luminescent carbon dot nanomaterials of helical superstructures for circularly polarized light detection. Adv Opt Mater 2018;6:1801246.
[54] Han YX, Lv WJ, Chen HL, Li H, Chen J, Li Z, Qiu HD. Chiral fluorescent silicon nanoparticles for aminopropanol enantiomer: fluorescence discrimination and mechanism identification. Anal Chem 2020;92:3949–57.
[55] Sujith M, Vishnu EK, Sappati S, Hassan MSO, Vijayan V, Thomas KG. Ligand-induced ground- and excited-state chirality in SiliconNanoparticles: surface interactions matter. J Am Chem Soc 2022;144:5074–86.
[56] Wang XB, Wang QS, Zhang XY, Miao J, Cheng JJ, He TC, Li YW, Tang ZK, Chen R. Circularly polarized light source from self-assembled hybrid nanoarchitecture. Adv Opt Mater 2022;10:2200761.
[57] Doring A, Ushakova E, Rogach AL. Chiral carbon dots: synthesis, optical properties, and emerging applications. Light Sci Appl 2022;11:75.
[58] Di Noja S, Amato F, Zinna F, Di Bari L, Ragazzon G, Prato M. Transfer of axial chirality to the nanoscale endows carbon nanodots with circularly polarized luminescence. Angew Chem Int Ed 2022;61:e202202397.
[59] Zhang ZW, Yang CJ, Dai YK, Zhang XY, Chen JQ, Feng LY. Circularly polarized luminescence of achiral carbon dots in Bi-solvent systems triggered by supramolecular self-assembly. Chem Eur J 2022:e202202589.
[60] Xu MC, Wu XY, Yang Y, Ma CH, Li W, Yu HP, Chen ZJ, Li J, Zhang K, Liu SX. Designing hybrid chiral photonic films with circularly polarized room-temperature phosphorescence. ACS Nano 2020;14:11130–9.
[61] Kang S, Biesold GM, Lee H, Bukharina D, Lin ZQ, Tsukruk VV. Dynamic chiro-optics of bio-inorganic nanomaterials via seamless Co-assembly of semiconducting nanorods and polysaccharide nanocrystals. Adv Funct Mater 2021;31:2104596.
[62] Bishop KJM, Wilmer CE, Soh S, Grzybowski BA. Nanoscale forces and their uses in self-assembly. Small 2009;5:1600–30.
[63] Wang JJ, Zhou HT, Yang JN, Feng LZ, Yao JS, Song KH, Zhou MM, Jin S, Zhang GZ, Yao HB. Chiral phosphine-copper iodide hybrid cluster assemblies for circularly polarized luminescence. J Am Chem Soc 2021;143:10860–4.
[64] Shi L, Zhu LY, Guo J, Zhang LJ, Shi YN, Zhang Y, Hou K, Zheng YL, Zhu YF, Lv JW, Liu SQ, Tang ZY. Self-assembly of chiral gold clusters into crystalline nanocubes of exceptional optical activity. Angew Chem Int Ed 2017;56:15397–401.
[65] Shi N, Tan JY, Wan XH, Guan Y, Zhang J. Induced salt-responsive circularly polarized luminescence of hybrid assemblies based on achiral Eu-containing polyoxometalates. Chem Commun 2017;53:4390–3.
[66] Ji LK, Zhao Y, Tao M, Wang HX, Niu D, Ouyang GH, Xia AD, Liu MH.

Dimension-tunable circularly polarized luminescent nanoassemblies with emerging selective chirality and energy transfer. ACS Nano 2020;14:2373–84.
[67] Yuan YX, Hu M, Zhang KR, Zhou TT, Wang S, Liu MH, Zheng YS. The largest CPL enhancement by further assembly of self-assembled superhelices based on the helical TPE macrocycle. Mater Horiz 2020;7:3209–16.
[68] Han Z, Zhao XL, Peng P, Li S, Zhang C, Cao M, Li K, Wang ZY, Zang SQ. Intercluster aurophilicity-driven aggregation lighting circularly polarized luminescence of chiral gold clusters. Nano Res 2020;13:3248–52.
[69] Yang JG, Li K, Wang J, Sun SS, Chi WJ, Wang C, Chang XY, Zou C, To WP, Li MD, Liu XG, Lu W, Zhang HX, Che CM, Chen Y. Controlling metallophilic interactions in chiral gold(I) double salts towards excitation wavelength-tunable circularly polarized luminescence. Angew Chem Int Ed 2020;59:6915–22.
[70] Huang JH, Wang ZY, Zang SQ, Mak TCW. Spontaneous resolution of chiral multi-thiolate-protected Ag-30 nanoclusters. ACS Cent Sci 2020;6:1971–6.
[71] Maeda T, Mori T, Ikeshita M, Ma SC, Muller G, Ariga K, Naota T. Vortex flow-controlled circularly polarized luminescence of achiral Pt(II) complex aggregates assembled at the air-water interface. Small Methods 2022;6.
[72] Arteaga O, Canillas A, Crusats J, El-Hachemi Z, Llorens J, Sacristan E, Ribo JM. Emergence of supramolecular chirality by flows. ChemPhysChem 2010;11:3511–6.
[73] Akine S, Miyake H. Stimuli-responsive chirality inversion of metallohelices and related dynamic metal complexes. Coord Chem Rev 2022:468.
[74] Yang H, Yuan B, Zhang X, Scherman OA. Supramolecular chemistry at interfaces: host-guest interactions for fabricating multifunctional biointerfaces. Acc Chem Res 2014;47:2106–15.
[75] Zhai R, Xiao YH, Gu ZG, Zhang J. Tunable chiroptical application by encapsulating achiral lanthanide complexes into chiral MOF thin films. Nano Res 2022;15:1102–8.
[76] Zhang C, Li ZS, Dong XY, Niu YY, Zang SQ. Multiple responsive CPL switches in an enantiomeric pair of perovskite confined in lanthanide MOFs. Adv Mater 2022;34:2109496.
[77] Xiao YH, Weidler P, Lin SS, Woll C, Gu ZG, Zhang J. Chiral metal-organic cluster induced high circularly polarized luminescence of metal-organic framework thin film. Adv Funct Mater 2022;32.
[78] Oliveira ON, Caseli L, Ariga K. The past and the future of Langmuir and Langmuir-blodgett films. Chem Rev 2022;122:6459–513.
[79] Gorbachev IA, Smirnov AV, Glukhovskoy EG, Kolesov VV, Ivanov GR, Kuznetsova IE. Morphology of mixed Langmuir and Langmuir-schaefer monolayers with covered CdSe/CdS/ZnS quantum dots and arachidic acid. Langmuir 2021;37:14105–13.
[80] Lv JW, Hou K, Ding DF, Wang DW, Han B, Gao XQ, Zhao M, Shi L, Guo J, Zheng YL, Zhang X, Lu CG, Huang L, Huang W, Tang ZY. Gold nanowire chiral ultrathin films with ultrastrong and broadband optical activity. Angew Chem Int Ed 2017;56:5055–60.
[81] Lv JW, Ding DF, Yang XK, Hou K, Miao X, Wang DW, Kou BC, Huang L, Tang ZY. Biomimetic chiral photonic crystals. Angew Chem Int Ed 2019;58:7783–7.
[82] Yang XK, Lv JW, Zhang J, Shen TX, Xing TY, Qi FL, Ma SH, Gao XQ, Zhang W, Tang ZY. Tunable circularly polarized luminescence from inorganic chiral photonic crystals doped with quantum dots. Angew Chem Int Ed 2022;61:e202201674.
[83] Chen LJ, Hao CL, Cai JR, Chen C, Ma W, Xu CL, Xu LG, Kuang H. Chiral self-assembled film from semiconductor nanorods with ultra-strong circularly polarized luminescence. Angew Chem Int Ed 2021;60:26276–80.
[84] Song FY, Xu Z, Zhang QS, Zhao Z, Zhang HK, Zhao WJ, Qiu ZJ, Qi CX, Zhang H, Sung HHY, Williams ID, Lam JWY, Zhao ZJ, Qin AJ, Ma DG, Tang BZ. Highly efficient circularly polarized electroluminescence from aggregation-induced emission luminogens with amplified chirality and delayed fluorescence. Adv Funct Mater 2018;28:1800051.
[85] Zinna F, Pasini M, Galeotti F, Botta C, Di Bari L, Giovanella U. Design of lanthanide-based OLEDs with remarkable circularly polarized electroluminescence. Adv Funct Mater 2017;27:1603719.
[86] Duan TW, Ai J, Chen SJ, He GF, Guo XJ, Han L, et al. Chiral CdSe/CdS quantum dot (in rod)-light-emitting diodes with circularly polarized electroluminescence. Nano Res 2022;15:9573–7.
[87] Wu ZG, Han HB, Yan ZP, Luo XF, Wang Y, Zheng YX, Zuo JL, Pan Y. Chiral octahydro-binaphthol compound-based thermally activated delayed fluorescence materials for circularly polarized electroluminescence with superior EQE of 32.6% and extremely low efficiency roll-off. Adv Mater 2019;31:1900524.
[88] Fang XN, Zheng YZ, Duan YK, Liu Y, Zhong WW. Recent advances in design of fluorescence-based assays for high-throughput screening. Anal Chem 2019;91:482–504.
[89] Imai Y, Nakano Y, Kawai T, Yuasa J. A smart sensing method for object identification using circularly polarized luminescence from coordination-driven self-assembly. Angew Chem Int Ed 2018;57:8973–8.
[90] Li W, Xu MC, Ma CH, Liu YS, Zhou J, Chen ZJ, Wang YG, Yu HP, Li J, Liu SX. Tunable upconverted circularly polarized luminescence in cellulose nanocrystal based chiral photonic films. ACS Appl Mater Interfaces 2019;11:23512–9.
[91] Kasprzyk-Hordern B. Pharmacologically active compounds in the environment and their chirality. Chem Soc Rev 2010;39:4466–503.
[92] Zhang NN, Sun HR, Liu SH, Xing YC, Lu J, Peng F, Han CL, Wei ZL, Sun TM, Yang B, Liu K. Gold nanoparticle enantiomers and their chiral-morphology dependence of cellular uptake. CCS Chemistry 2022;4:660–70.
[93] Zhao TH, Han JL, Jin X, Liu Y, Liu MH, Duan PF. Enhanced circularly polarized luminescence from reorganized chiral emitters on the skeleton of a zeolitic imidazolate framework. Angew Chem Int Ed 2019;58:4978–82.
[94] Wang Q, Lin BY, Chen M, Zhao CX, Tian H, Qu DH. A dynamic assembly-induced emissive system for advanced information encryption with time-dependent security. Nat Commun 2022;13:4185.
[95] Xu MC, Ma CH, Zhou J, Liu YS, Wu XY, Luo S, Li W, Yu HP, Wang YG, Chen ZJ, Li J, Liu SX. Assembling semiconductor quantum dots in hierarchical photonic cellulose nanocrystal films: circularly polarized luminescent nanomaterials as optical coding labels. J Mater Chem C 2019;7:13794–802.
[96] Juan A, Sun H, Qiao JH, Guo JB. Near-infrared light-controlled circularly polarized luminescence of self-organized emissive helical superstructures assisted by upconversion nanoparticles. Chem Commun 2020;56:13649–52.
[97] Richardson RD, Baud MGJ, Weston CE, Rzepa HS, Kuimova MK, Fuchter MJ. Dual wavelength asymmetric photochemical synthesis with circularly polarized light. Chem Sci 2015;6:3853–62.
[98] Yang G, Zhu LF, Hu JG, Xia HY, Qiu D, Zhang QJ, Zhang DG, Zou G. Near-infrared circularly polarized light triggered enantioselective photopolymerization by using upconversion nanophosphors. Chem Eur J 2017;23:8032–8.
[99] Zhang MM, Dong XY, Wang ZY, Li HY, Li SJ, Zhao XL, Zang SQ. AIE triggers the circularly polarized luminescence of atomically precise enantiomeric copper(I) alkynyl clusters. Angew Chem Int Ed 2020;59:10052–8.
[100] Frawley AT, Pal R, Parker D. Very bright, enantiopure europium(III) complexes allow time-gated chiral contrast imaging. Chem Commun 2016;52:13349–52.
[101] Stachelek P, MacKenzie L, Parker D, Pal R. Circularly polarised luminescence laser scanning confocal microscopy to study live cell chiral molecular interactions. Nat Commun 2022;13:553.

Xiongbin WANG received his bachelor's degree in Department of Electrical and Electronic Engineering, Southern University of Science and Technology. He is now a joint Ph.D candidate at Institute of Applied Physics and Materials Engineering, University of Macau, and Department of Electrical and Electronic Engineering, Southern University of Science and Technology under the supervision of Prof. Zikang Tang and Prof. Rui Chen. His current research interests focus on investigating optical activity of emerging chiral nanomaterials and their novel applications.

Rui CHEN received his PhD degree in applied physics from Nanyang Technological University, and physics from Xiamen University. He is currently working at the Department of Electrical and Electronic Engineering at Southern University of Science and Technology. His research interests include the laser spectroscopy, optical properties of materials, optical microcavity and micro/nano lasers.